Hydraulic Characterization of Hydrothermally Altered Nopal Tuff

Prepared by
R. T. Greene, G. Rice, K. A. Meyer-James

Southwest Research Institute
Center for Nuclear Waste Regulatory Analyses

Hydraulic Characterization of Hydrothermally Altered Nopal Tuff

Prepared by
R. T. Green, G. Rice*, K. A. Meyer–James

Southwest Research Institute
Center for Nuclear Waste Regulatory Analyses
6220 Culebra Road
San Antonio, TX 78228–0510

*Consultant, George Rice and Associates, San Antonio, TX

ABSTRACT

Understanding the mechanics of variably saturated flow in fractured-porous media is of fundamental importance to evaluating the isolation performance of the proposed high-level radioactive waste repository for the Yucca Mountain site. Developing that understanding must be founded on the analysis and interpretation of laboratory and field data. This report presents an analysis of the unsaturated hydraulic properties of tuff cores from the Peña Blanca natural analog site in Mexico. The basic intent of the analysis was to examine possible trends and relationships between the hydraulic properties and the degree of hydrothermal alteration exhibited by the tuff samples. These data were used in flow simulations to evaluate the significance of a particular conceptual (composite) model and of distinct hydraulic properties on the rate and nature of water flow.

CONTENTS

CONTENTS (Cont'd)

FIGURES

FIGURES (Cont'd)

TABLES

NOMENCLATURE

A_w = water activity coefficient (-)
G_{app} = apparent specific gravity
G_{bulk} = bulk specific gravity
G_{SSD} = bulk specific gravity

K_{sat} = saturated hydraulic conductivity (cm/s)
K_f = fracture hydraulic conductivity (m/s)
k_f = fracture permeability

M_{dry} = dry mass (g)
M_{sat} = saturated mass (g)

n_{eff} = effective porosity

P_c = sample chamber volumes (cm^3)
P_f = final pressure
P_r = gas pressure

R/M   = gas constant/molecular mass of water (4.61 mPa/c)

V_c = sample chamber volumes (cm^3)
V_r = volume of reservoir (cm^3)
V_s = volume sample (cm^3)

wt_{dry} = dry sample weight (g)
wt_{read} = sample weight at a particular matric potential (g)
wt_{sat} = saturated sample weight (g)

Greek

ρ_b = sample bulk density (g/cm^3)

ρ_w = density of water (g/cm3)

ψ = ma.. potential (Pa)

ϕ = fracture porosity

NOMENCLATURE (Cont'd)

A = cross sectional curve of sample (m^3)

h = difference in hydraulic head across sample (mH_2O)

k = hydraulic conductivity (m/s)

L = length of sample along which flow occur (m)

q = quantity of flow taken as average of in flow and out flow (m^3)

S = sample percent saturation (-)

t = interval of test time (s)

ACKNOWLEDGMENTS

QUALITY OF DATA, ANALYSES, AND CODES

DATA: CNWRA-generated data contained in this report meet quality assurance requirements described in the CNWRA Quality Assurance Manual. Sources for other data cited in the report should be consulted for determining the level of quality for those data.

ANALYSES AND CODES: The V-TOUGH code is controlled under the CNWRA Software Configuration Procedure. The RETC code is not currently under software configuration management. Testing is underway to bring RETC into compliance with the software configuration management procedures.

LIST OF ABBREVIATIONS

ABBREVIATION	DESCRIPTION
1D, 2D	1-Dimensional, 2-Dimensional
ASTM	American Society for Testing and Materials
CNWRA	Center for Nuclear Waste Regulatory Analyses
DOE	U.S. Department of Energy
EPRI	Electric Power Research Institute
HLW	High-Level Radioactive Waste
IPAs	Iterative Performance Assessments
KTUs	Key Technical Uncertainties
LA	License Application
LARP	License Application Review Plan
NRC	U.S. Nuclear Regulatory Commission
PA	Performance Assessment
PACs	Potentially Adverse Conditions
TSPAs	Total-System Performance Assessments
U	Uranium
YM	Yucca Mountain

1 INTRODUCTION

1.1 REGULATORY NEED

Predictive analyses of water flow in fractured-porous tuff will play a central role in the evaluation of Yucca Mountain (YM), in southwest Nevada, as a potential high-level radioactive waste (HLW) repository site. Faults and well interconnected fracture systems in YM are likely to be the predominant conduits for water movement from the surface to the repository horizon and, ultimately, to the water table. Although the arid climate of the YM site is very favorable to waste isolation, observations of water flow in tunnels at the nearby Rainier Mesa (Russell et al., 1988), for example, indicate that fractures may serve as major conduits in the fractured tuff. In addition to promoting fluid ingress to the repository, faults and fractures may also act as fast pathways through the geologic barrier.

Iterative performance assessments (IPAs) for the YM site have been conducted by the U.S. Nuclear Regulatory Commission (NRC) (U.S. Nuclear Regulatory Commission, 1992; 1995). Sensitivity analyses conducted as part of these IPAs have consistently indicated that infiltration, along with the associated deep percolation through the fractured-porous tuff, is a critical factor controlling the isolation performance of the proposed repository. A similar finding has been noted in total-system performance assessments (TSFAs) conducted by the U.S. Department of Energy (DOE) researchers (Sandia National Laboratories, 1992; 1994) and those of the Electric Power Research Institute (EPRI) (Electric Power Research Institute, 1990; 1992). This consistent finding is particularly noteworthy in view of the fact that NRC, DOE, and EPRI have utilized relatively distinct assumptions and approaches to model the water flow through the unsaturated, fractured-porous tuff formations of the YM site.

While noting the importance of fracture flow in performance assessment (PA), it is also necessary to acknowledge that there are major uncertainties in mathematically modeling the process of variably saturated flow in fractures, as well as the matrix-fracture interactions. These uncertainties have been noted in the technical literature and by a DOE peer-review panel (Freeze, 1991). NRC sponsored research at the Center for Nuclear Waste Regulatory Analyses (CNWRA) has begun to examine this fluid flow phenomenon through the use of basic fluid dynamics approaches (Kapoor, 1994), laboratory studies of a single fracture (Mohanty, 1994), and the analysis of field data from the Peña Blanca natural analog site in Mexico (Pearcy, 1994). NRC sponsors other research on flow through fractures at the University of Arizona.

The NRC staff needs to develop a capability to model water flow in unsaturated, fractured-porous tuff in order to evaluate the DOE assessments of the postclosure performance of the proposed repository, in accordance with the NRC regulation 10 CFR Part 60. These technical evaluations are expected to benefit such regulatory activities as:

- Evaluating key technical uncertainties (KTUs) identified in the NRC License Application Review Plan (LARP) (U.S. Nuclear Regulatory Commission, 1993)

- Reviewing and commenting on the DOE and TSPAs (Sandia National Laboratories, 1992; 1994)

- Making determinations regarding the adequacy of the DOE demonstrations of compliance in the License Application (LA)

The experience gained from these evaluations will also be used in developing guidance for the DOE on various aspects of PA.

1.2   OBJECTIVES AND SCOPE

The study documented in this report was performed through the integration of technical activities conducted under two NRC-sponsored research projects, namely the PA Research Project and the Geochemical Natural Analog Project. The collection and laboratory measurement of intrinsic and hydraulic properties of tuff cores were performed under the auspices of the Geochemical Natural Analog Project. The analysis of laboratory data and its preliminary use in modeling infiltration at the Peña Blanca natural analog site were performed under the PA Research Project. Consequently, this report constitutes an integration product of coordinated and integrated research on flow in fractured-porous tuff.

One of the main objectives of this study was to examine the possible importance of hydrothermal alteration on the unsaturated hydraulic properties of the tuff. It was hypothesized that hydraulic properties, such as the saturated hydraulic conductivity and moisture retention curve, might vary significantly depending on the degree of hydrothermal alteration (Flint et al., 1994). Detailed measurements of these and other properties (e.g., porosity, bulk density, and specific gravity) for five tuff samples were analyzed to identify trends and relationships. These properties were input to a flow simulation code, V-TOUGH, to model a proposed infiltration experiment at the Peña Blanca site. These simulations provided a basis for judging the possible significance of the distinct properties on the rate and nature of water movement.

1.3   REPORT CONTENT

This technical report is organized into six major chapters. Chapter 1 serves as the introduction to the study, while Chapter 2 presents general background information on the Peña Blanca site with emphasis on describing the particular formation from which the samples were taken. Chapter 3 outlines the specific physical and hydraulic properties that were measured, as well as the laboratory procedures used in their measurement. Chapter 4 summarizes the actual data and the analysis of data in tabular form, including appropriate statistical parameters. In Chapter 5, a series of flow simulations is presented, graphically compared, and evaluated. The final chapter, Chapter 6, presents the technical findings of the study and outlines specific recommendations for further field and modeling studies of fracture flow at the Peña Blanca site. The full set of data collected in this study is attached in Appendices A through E, which are appended as microfiche to this report.

2 BACKGROUND

2.1 GENERAL GEOLOGY

The Peña Blanca natural analog site is located at the Nopal I uranium (U) deposit in Chihuahua City, Mexico. It is part of the Sierra Peña Blanca, which lies approximately 50 km north of Chihuahua City, Mexico (Figure 2-1). The Sierra Peña Blanca is a horst block of the Basin and Range type that is about 80 km in length and 15 to 20 km wide. It consists of Mesozoic and Cenozoic rocks underlain by a series of Cretaceous limestones. The Sierra Peña Blanca has an average elevation of about 1,800 m, rising a full 200 m above the surrounding basins (George-Aniel et al., 1991). It strikes generally north with a westward tilt. The east side of the Sierra Peña Blanca has been designated as the boundary between the Chihuahua trough to the east and the Aldama platform to the west. Further to the east, it is bounded by the Chihuahua tectonic belt (Goodell, 1981). Superimposed on the Sierra Peña Blanca is a set of northwest striking normal faults (Pearcy and Murphy, 1992).

The Nopal Formation has been dated at 44 million yr (Alba and Chavez, 1974). At the Nopal 1, the formation consists of two members, an upper highly welded rhyolitic tuff and a lower ash flow tuff (Ildefonse et al., 1990). Hydrothermal fluids transporting U appear to have moved up through a breccia pipe and outward along fault and fracture traces. Currently the regional water table is at a depth of greater than 200 m (Pearcy et al., 1994).

2.2 SAMPLE COLLECTION AND IDENTIFICATION TECHNIQUES

An initial set of four tuff samples was collected from the Peña Blanca natural analog site at the Nopal I deposit. These samples were collected to permit evaluation of tuffs exhibiting varying degrees of hydrothermal alteration, in this case, associated with the U deposit located in a brecciated zone. The samples are designated as NRG1 through NRG4. The degree of alteration in the samples ranges from the highly altered rock located at the edge of the brecciated zone, NRG1, to the unaltered host rock, NRG4. Sample NRG2 is located at a distance of 18 m from the deposit, with NRG3 located at a distance of 50 m, exhibiting less alteration. Sample NRG4 is located at a horizontal distance of about 400 m. A fifth rock sample, NRG5, was collected at a horizontal distance of 22 m when it became apparent that the degree of alteration between samples NRG2 and NRG3 was large and that NRG3 exhibited properties similar to NRG4, presumed to represent the unaltered host rock. The sample sequence from most altered to least altered is, thereby, NRG1, NRG2, NRG5, NRG3, and NRG4 (Figure 2-2).

A series of subsamples (dissected cores) was prepared from each rock sample for laboratory hydraulic characterization experiments. Each series consisted of samples cut from multiple rock cores taken at three different core dimensions oriented at three orthogonal directions in the rock sample. The subsamples were cored from the five rock samples using a rock drill with tap water as the drilling fluid.

Each subsample is identified by three sets of designators separated by asterisks, for example, NRG1*BXY*1. The first set of designators identifies the original tuff sample from which the subsamples were taken (NRG1, NRG2, NRG5, NRG3, and NRG4). The next set of designators identifies the core size (i.e., core diameter) and relative orientation of the core (e.g., BXY). The sizes are identified as A, B, and C with diameters equal to 1.90, 5.01, and 7.64 cm, respectively. Orientation of each of the five rock samples
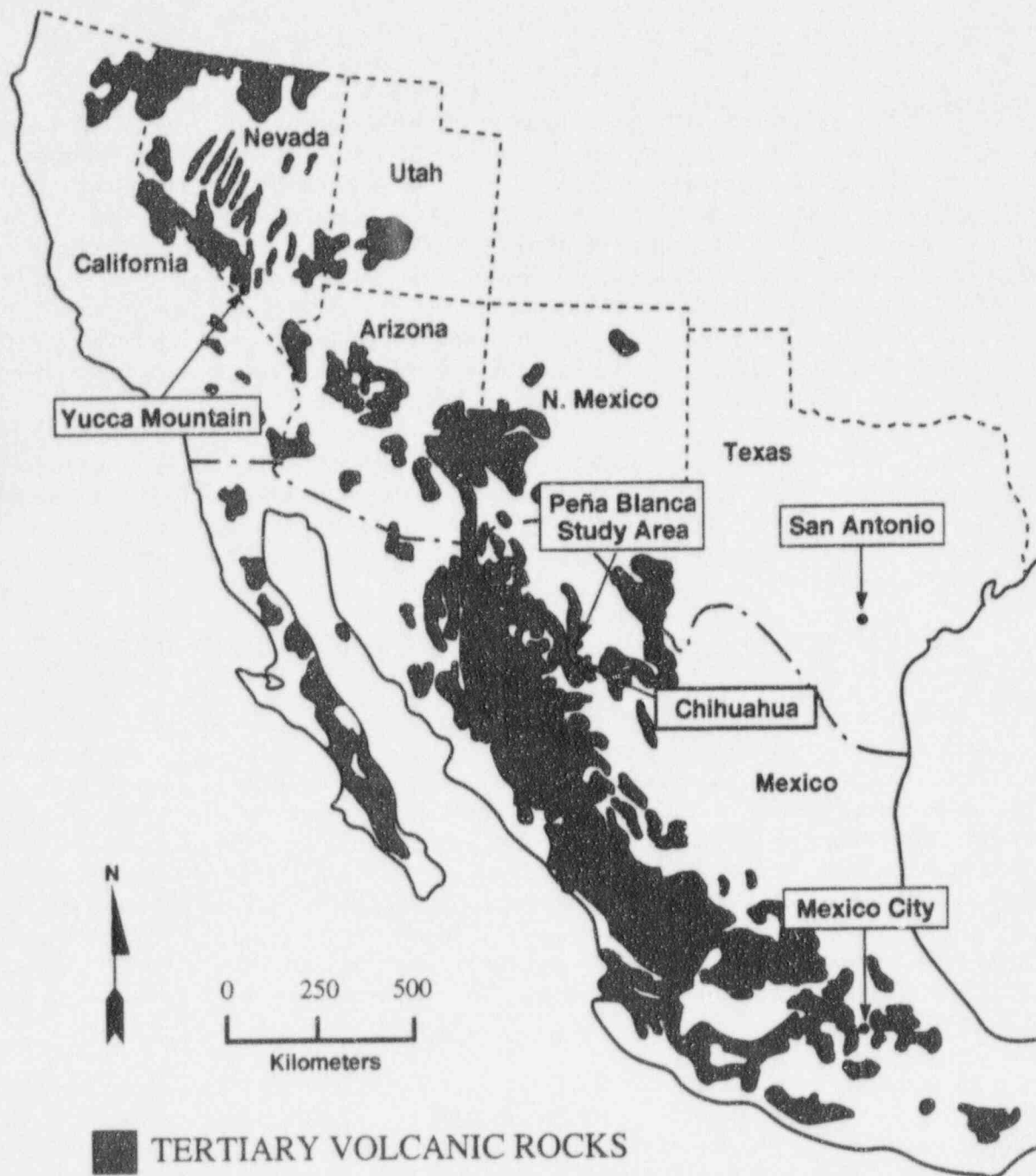
Figure 2-1. The Nopal I uranium deposit is located in the Peña Blanca mining district, Chihuahua, Mexico. Yucca Mountain, Nevada, the proposed site for the U.S. high-level waste repository, is located northwest of the Peña Blanca District along a general trend of Tertiary volcanic rocks in the Basin and Range province.
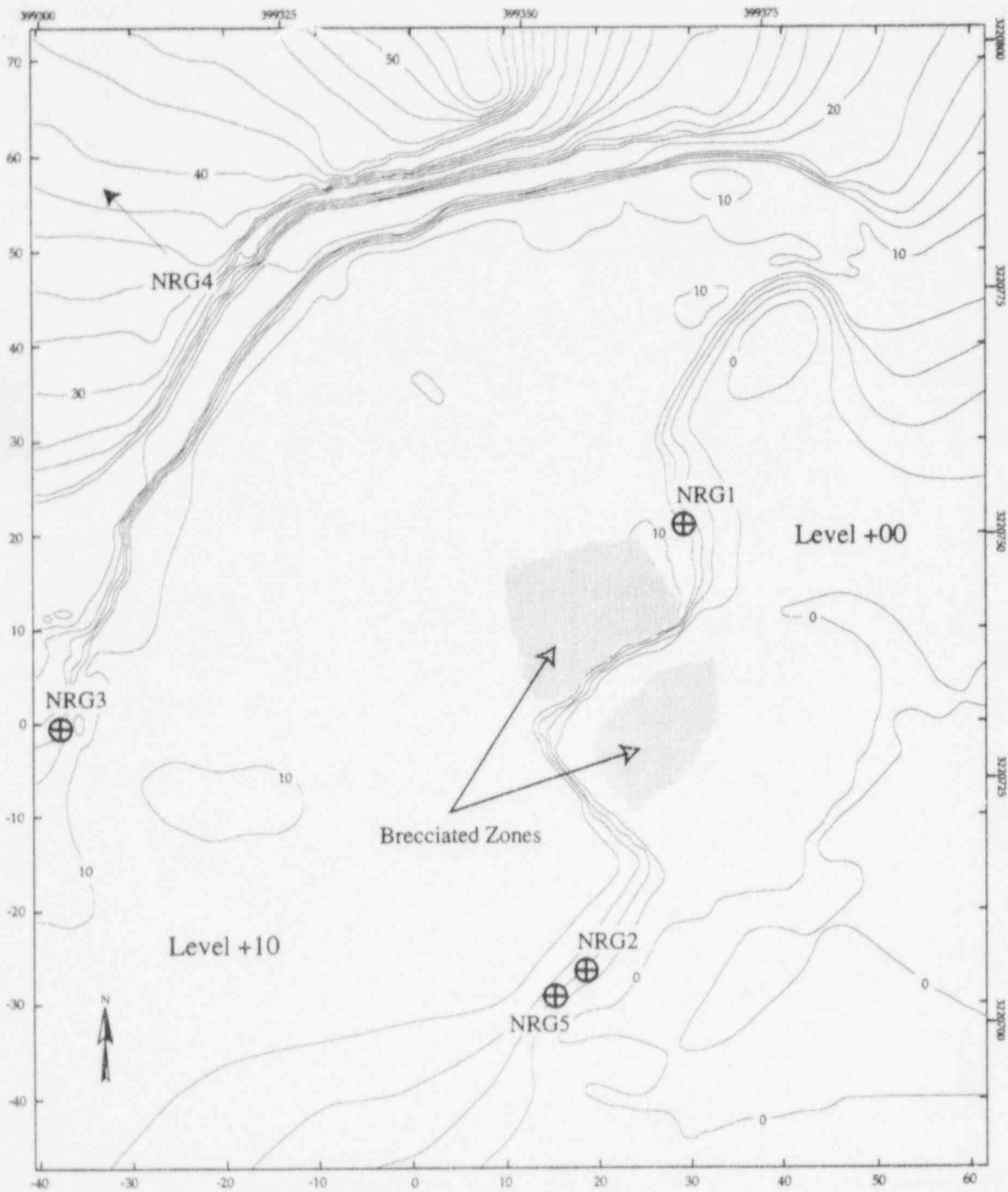
Figure 2-2. Collection sites of the Nopal tuff samples. Contour map by E. Pearcy based on original planetable mapping by I. Reyes. NRG4 is located 400 m from edge of brecciated zone. Grid marks on left and bottom of figure are in meters.

NUREG/CR-6356

was arbitrarily determined relative to the elongation of vesicles in the original rock sample. The z-direction is orthogonal to the elongated direction of the vesicles, and xy- and yx-directions are at mutually perpendicular directions to z. The final set of designators is a number to indicate the sequential order of the subsample prepared from each core (i.e., the cores were cut or dissected into disk-shaped subsamples of varying lengths and sequentially numbered).

3 PROPERTY DETERMINATION METHODS

Matrix intrinsic and hydraulic properties of the five Nopal tuff samples were measured in the CNWRA laboratory over a period of 18 mo. Many of the testing procedures used in these analyses were originally designed for soils and had to be adapted to accommodate the highly welded and dense nature of the Nopal tuff samples.

3.1 MATRIX INTRINSIC PROPERTIES

The matrix intrinsic properties of the Nopal tuff samples were measured in the laboratory using standard testing procedures [e.g., American Society for Testing and Materials (ASTM), Methods of Soil Analysis, or other documented methodology]. The measured properties included bulk density, apparent specific gravity, bulk specific gravity, bulk specific gravity-saturated surface dry (SSD), and effective porosity. Although standard testing procedures were employed in the measurement of the matrix interstitial properties, these testing techniques were enhanced in the CNWRA laboratory to address specific difficulties arising from the particular nature of hydrothermally altered rock samples. The testing methodologies used to determine the matrix interstitial properties are described in the following subsections.

3.1.1 Bulk Density

Bulk density is defined as the dry mass (measured in g) of a sample divided by the sample volume (measured in cm^3) (Marshall and Holmes, 1988). The procedure was taken from Rasmussen et al. (1990) and consisted of placing the subsamples in an oven at 105 °C and drying until a constant mass was reached. Constant mass was defined as three consecutive measurements within 0.002 g. The subsamples were then placed in a desiccator and allowed to cool to room temperature, at which time the mass of each was measured with a calibrated Mettler PM480 electronic balance with a deviation of ±0.003 g. The volumes of the subsamples were determined by measuring their dimensions via a caliper to the nearest 1/100 of a cm. Bulk density of each subsample was thus:

$$\rho_b = \frac{M_{dry}}{V} \tag{3-1}$$

where:

ρ_b = sample bulk density (g/cm^3)

M_{dry} = dry mass (g)

V = sample volume (cm^3)

Using this methodology, the bulk densities of a total of 289 subsamples were measured on 46, 52, 71, 70, and 50 subsamples taken from the tuff samples NRG1, NRG2, NRG3, NRG4, and NRG5,

ectively. A complete listing of all subsamples tested for bulk density including subsample volumes and weights is included in Appendix A.

3.1.2 Specific Gravity

Specific gravity is defined as the density or specific weight of a unit volume to the mass of an equal volume water (Freeze and Cherry, 1979). Types of specific gravity measured include: (i) apparent specific gravity, (ii) bulk specific gravity, and (iii) bulk specific gravity SSD. Apparent specific gravity (G_{app}) is defined in American Society for Testing and Materials (1993) as the ratio of the weight in air of the impermeable portion of a unit volume to the mass of and equal volume of deaired deionized water at the same temperature. Apparent specific gravity applies to the relative density of the matrix material not including the permeable pore space. This parameter is analogous to skeletal density as defined by Rasmussen et al. (1990).

Bulk specific gravity (G_{bulk}) is defined as the ratio of the mass of a unit volume, including effective and ineffective porosity, to an equal volume of deaired deionized water (American Society for Testing and Materials, 1993). It represents the specific gravity of a sample as it would exist above the water table. As defined here, bulk specific gravity was termed unsaturated specific gravity by Carrier (1979), mass specific gravity by Sowers (1979), but is referred to as apparent specific gravity by Krynine and Judd (1951).

Alternately, bulk specific gravity (G_{SSD}) also is defined as the saturated weight of a unit volume, compared to an equal volume of deaired deionized water (American Society for Testing Materials, 1993). This parameter measures the specific gravity of a sample as it would exist below the water table and was termed saturated specific gravity by Carrier (1979). It is analogous to the dry bulk density of Hillel (1971) and the bulk density of Rasmussen et al. (1990).

The basic testing methods for the three types of specific gravity measurements were adapted from American Society for Testing Materials, (1993), American Soceity for Testing Materials (1990), and Carrier (1979). First, the masses of the oven-dried subsamples were determined as described in Section 3.1.1. Next, the subsamples were saturated using the following procedures. The subsamples were placed in a hermetically sealed vessel, and air was evacuated with a vacuum pump capable of pulling a vacuum of −0.8 bar (a calibrated Dwyer™ handheld manometer was used to determine the capability of the pump). CO_2 was introduced into the vessel at a pressure of approximately 0.7 bar for 1 min after which the vacuum was redrawn. The vacuum-CO_2 cycle was repeated twice. After completion of the cycle, the subsamples were left in the vacuum for 24 hr. Sufficient deaired, deionized water (with an assumed specific gravity of 1.000 at laboratory temperatures) was allowed to enter the vessel to cover the subsamples. The subsamples were then left in the water-filled chamber under vacuum for 24 hr to saturate the subsample. The saturated masses of the subsamples were measured with the Mettler PM480 electronic balance while suspended in deaired deionized water. Each subsample was then patted dry with a damp towel so no free water coated the surface. Their saturated mass in air was measured with the Mettler balance. The bulk volume of the subsample was calculated as the saturated mass in air minus the saturated mass in water. The specific gravities, G, of the subsamples were determined by the following equations:

$$G_{app} = \frac{M_{dry\ in\ air}}{M_{dry\ in\ air} - M_{sat\ in\ water}},$$ (3-2)

$$G_{bulk} = \frac{M_{dry\ in\ air}}{M_{sat\ in\ air} - M_{sat\ in\ water}}$$ (3-3)

$$G_{SSD} = \frac{M_{sat\ in\ air}}{M_{sat\ in\ air} - M_{sat\ in\ water}}$$ (3-4)

The three types of specific gravity were measured for a total of 274 subsamples with 46, 51, 70, 70, and 37 subsamples taken from the sample groups NRG1, NRG2, NRG3, NRG4, and NRG5, respectively. A complete listing of all specific gravity measurements including sample dry masses, saturated masses in air, and saturated masses in water is included in Appendix B.

3.1.3   Effective Porosity

Effective porosity is defined as the volume of interconnected voids per unit bulk volume of solids. Two basic methods were used to determine the effective porosity of the subsamples, that is, the gravimetric method and the gas pycnometer method. The two procedures used to conduct the porosity experiments are described in the following subsections.

3.1.3.1   Gravimetric Method

The gravimetric method of measuring effective porosity was adapted from Rasmussen et al. (1990). The theory of the gravimetric method is to equate porosity to the difference in mass between a saturated and an oven-dried sample. The subsamples were initially dried in an oven at 105 °C per Section 3.1.1, and weighed on a Mettler PM480 electronic balance. Each subsample was then saturated as described in Section 3.1.2 with deaired, deionized water. Effective porosity, n_{eff}, was determined using the following equation:

$$n_{eff} = \frac{M_{sat} - M_{dry}}{\rho_w V}$$ (3-5)

where

ρ_w =   density of water.

A total of 284 subsamples was measured with 46, 51, 70, 70, and 47 subsamples taken from the sample groups NRG1, NRG2, NRG3, NRG4, and NRG5, respectively. The measured effective porosity values for all subsamples tested using the gravimetric method are listed in Appendix C.

3.1.3.2 Pycnometer Method

The gas pycnometer method for measuring porosity is based on Boyle's gas law, which states that, at constant temperature, the product of the pressure and the volume of a gas for a contained system is a constant. Therefore, if a quantity of a gas at a known volume and pressure is allowed to expand into a larger volume (initially at atmospheric pressure), the resulting pressure can be used to calculate the new volume (Page, 1948; Russell, 1950) by equating the sum of the pressure-volume products to the combined system.

$$V_c P_c + V_r P_r = (V_c + V_r) P_f \tag{3-6}$$

where

V_c = the sample chamber volume (cm^3)

P_c = the sample chamber pressure (bar)

V_r = initial known volume of gas in the reservoir (cm^3)

P_r = initial known gas pressure of the reservoir (bar)

P_f = final gas pressure of the combined system (bar)

The volume of the sample is thereby the difference in the sample chamber volume measurements conducted with and without the sample.

The specific gas pycnometer methodology used to measure effective porosity of the Nopal subsamples was modified from Methods of Soil Analysis Part 1 (1986). To apply the principle of Boyle's gas law, a constant volume pycnometer, such as the one mentioned in the monograph by Danielson and Southerland (1986), was assembled. Details of the constant volume gas pycnometer are illustrated in Figure 3-1. The apparatus consists of two chambers, a sample chamber and a reservoir, both of which are wrapped by copper tubing through which a constant temperature bath circulates water to maintain the two chambers at a constant temperature—usually slightly above ambient or about 25 °C. These chambers can be isolated or connected as needed by a ball valve. A calibrated hand-held Dwyer series 475 Mark II digital manometer capable of measuring to the nearest 1/100 of 1 psi (6.895×10^{-4} bar) was used to measure the pressure within the system during the analysis.

The constant volume gas pycnometer measurement procedure is as follows. The volume of the reservoir chamber (V_r) was calculated from reservoir dimensions that were measured using a caliper. With the sample chamber empty, the valve between the chambers was opened, and gas (helium) was introduced into both the reservoir and the sample chamber to a known initial gas pressure (P_r), typically between 1.172 and 1.395 bar. The inflow valve was closed, and the chamber was stabilized for approximately 3 to 5 min to allow: (i) the gas to attain thermal equilibrium with the water bath, and (ii) to ensure there were no leaks in the system. The valve between the sample chamber and reservoir was then closed, isolating the reservoir at the initial pressure (P_r). The relief valve located on the sample chamber was opened, allowing the chamber to come to atmospheric pressure. The relief valve was then closed, and the
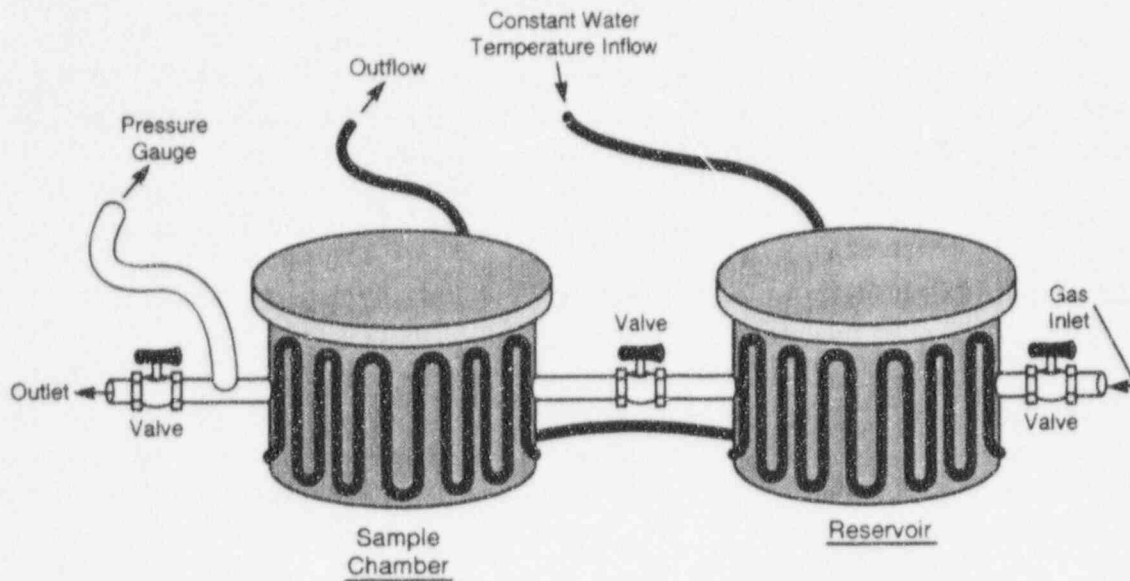
Figure 3-1. Schematic of a constant volume gas pycnometer used to measure porosity

two chambers were pneumatically connected by opening the valve between them. Once again, the system was allowed to sit for 3 to 5 min to ensure thermal equilibrium, after which the final pressure (P_f) of the combined system was recorded. Solving Eq. (3-6) for V_c, the volume of gas in the sample chamber was calculated as follows:

$$V_c = (P_r - P_f)\frac{V_r}{P_r} \tag{3-7}$$

The process was immediately repeated with an oven dried subsample (Section 3.1.2) of known volume (V_s) placed in the sample chamber, therefore changes in barometric pressure could be ignored. The difference in the two volumes is equivalent to the volume of solids in the subsample. Effective porosity was obtained by:

$$n_{\text{eff}} = \frac{V_c^{\text{without sample}} - V_c^{\text{with sample}}}{V_s} \tag{3-8}$$

Only the medium- and large-size subsamples (B and C) were measured for effective porosity using the gas pycnometer method. The total number of samples measured was 55, with 8, 10, 13, 13, and 11 subsamples from NRG1, NRG2, NRG3, NRG4, and NRG5, respectively. A complete listing of the measured gas pycnometric porosity values is included with the measured gravimetric effective porosity values in Appendix C.

3.2   MATRIX HYDRAULIC PROPERTIES

Laboratory analyses of the matrix hydraulic properties of the five Nopal tuff samples were conducted in the CNWRA laboratory. Hydraulic properties that were measured on these samples included the saturated hydraulic conductivity (K_{sat}) and the moisture characteristic curve. The large- and medium-diameter subsamples (size B and C) were used in the measurement of K_{sat}, and the small- and medium-diameter cores (size A and B) were used to determine the characteristic curve.

3.2.1   Saturated Hydraulic Conductivity

Saturated hydraulic conductivity was measured using a constant head permeameter, a Brainard Kilman S-480, and a S-510 flex-wall permeameter in conjunction with a Brainard Kilman control panel. The basic methodology was taken from American Society for Testing Materials (1990). The theory of the test is based on Darcy's law, in which it is assumed the flow is steady, one-dimensional (1D), and that the core is completely saturated.

The flex wall permeameter is illustrated in Figure 3-2. Saturated hydraulic conductivity is determined with the flex-wall permeameter by measuring the rate of flow through a media specimen by imposing a constant pressure differential across the specimen. A porous plate is placed at each end of the specimen to provide uniform pressures across each end of the specimen. The sample is maintained under a sufficiently high sidewall confining pressure to prevent short-circuit fluid flow along the sides of the sample (i.e., boundary flow). The integrity of the flex-wall permeameter was tested by demonstrating an absence of flow between the two porous plates when the sample was a disk of highly impermeable plastic.

The specific methodology used to measure saturated hydraulic conductivity is as follows. A saturated subsample (see Section 3.1.2) was confined between porous plates and filter paper, which were positioned on the top and bottom of the subsample as shown in Figure 3-2. Lengths of the subsamples used in these tests varied from 0.59 to 2.15 cm. Although subsamples with greater lengths are usually preferable, the low-hydraulic conductivities of samples exhibiting minimal or no alteration required long periods of time for sufficient measurement to be conducted. As a result, shorter subsamples were used. For example, a testing period of 8 mo at a pressure differential of about 4 bar would be required to obtain 1 cm^3 of permeant through a 5-cm diameter sample with a hydraulic conductivity of 2×10^{-12} m/s in accordance with American Society for Testing Materials (1990), which specifies that the height is equal to the diameter. Conversely, short subsamples provided for short-circuit pathways to form due to lithophysae or alteration products that are sufficiently large to bridge the length of the subsamples. Consequently, the sample lengths were determined by inspecting the individual samples for the absence of features that could provide for inappropriately short flow pathways. Filter paper was placed between the sample ends and porous plates to ensure adequate hydraulic connection. The combined subsample, filter paper, and porous plate assembly was placed between end plates and hermetically encased in an impermeable latex membrane and positioned inside the permeameter cell. The cell was sealed, and the annulus was filled with water. The annulus water in the permeameter cell was brought to and maintained at a pressure greater than the pressure to be imposed on the sample, with the result that the membrane was forced against the sidewalls of the sample to prevent flow of the permeant from one porous plate to the other except through the sample. A constant pressure head differential was then imposed across the sample. The permeant was deaired and deionized water. A 0.0525-percent solution of sodium hypochlorite was added to the water to

prevent biological plugging of pores. The quantity of permeant discharged through the sample was measured with respect to time. Saturated hydraulic conductivity was calculated using Darcy's law:

$$K = \left(\frac{q}{t}\right)\left(\frac{L}{Ah}\right) \qquad (3\text{-}9)$$

where:

K = hydraulic conductivity (m/s)

q = quantity of flow, taken as average of inflow and outflow (m^3)

t = interval of test time (s)

L = length of sample along which flow occurs (m)

A = cross-sectional area of sample (m^2)

h = difference in hydraulic head across sample [m H$_2$O]

Successive tests over a range of different hydraulic heads were performed on each subsample to demonstrate that the flow was steady and laminar during the tests. A total of 27 subsamples was tested for hydraulic conductivity by the constant head method, with 6, 6, 6, 5, and 4 subsamples from NRG1, NRG2, NRG3, NRG4, and NRG5, respectively. A table of saturated hydraulic conductivity values measured at each pressure differential for all subsamples is listed in Appendix D.

3.2.2 Moisture Retention Curve

The matric potential/saturation relationship, expressed here as moisture retention curves, was obtained for all five Nopal tuff samples using two methods, one for low matric potentials and the other at high matric potentials. Only the drying curve was measured in both methods. Low matric potentials (i.e., up to 15 bar), or relatively wet conditions, were measured with porous plate extractor methods. Subsamples at the dry end of the curve, with matric potentials as low as 10 bar to greater than 1,000 bar, were determined using a water activity meter. In both methods, the percent saturation of the subsample at a known matric potential was determined gravimetrically. Using a series of subsamples from each tuff sample, the measured matric potential/saturation relationship was used to construct the moisture retention curve for that sample. The two methods used to construct the retention curves are described in the following subsections.

3.2.2.1 Porous Plate Extractor Methods

The matric potential/saturation relationship at the low-saturation end of the moisture retention curves of the five Nopal samples was determined using a Soil Moisture porous plate extractor. The retention curve determination method was adapted from American Society for Testing Materials (1977), American Society for Testing Materials (1988), Klute (1986), and the manufacturer instructions. Using a porous plate extractor, the relationship between saturation and matric potential of a porous sample is
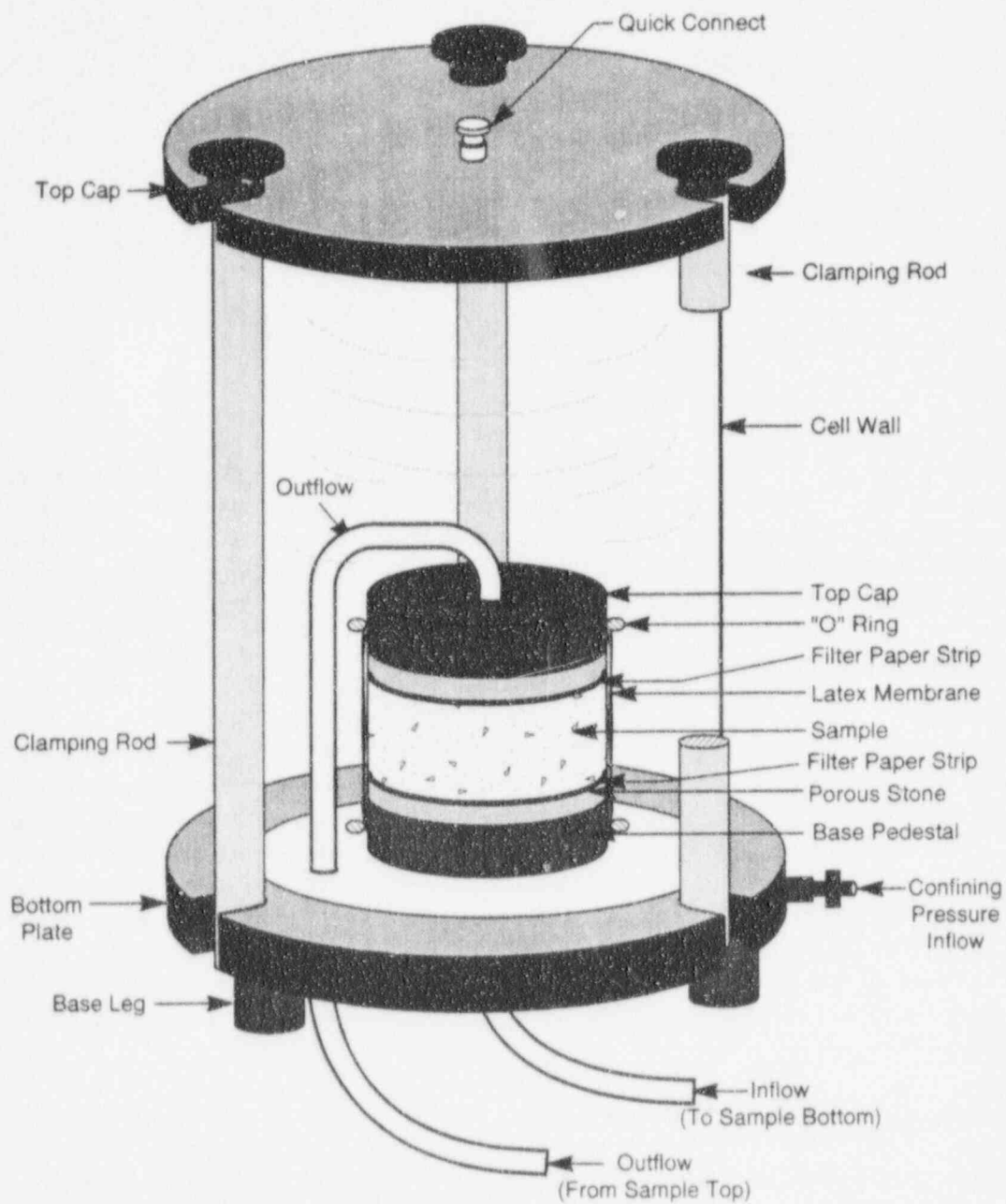
Figure 3-2. Schematic of a constant head permeameter used to measure saturated hydraulic conductivity

measured by applying a known positive pressure to dewater the sample, which is then gravimetrically weighed. Saturation at the specified pressure is determined using the change in weight relative to the fully saturated sample. The retention curve for the media sample is determined when a sufficient number of saturation measurements at known matric potentials is made. A Soil Moisture 15-bar pressure plate extractor has the advantage of being able to contain multiple subsamples, therefore allowing many measurements to be made simultaneously. The disadvantages of the pressure plate extractor method include: (i) problems determining when equilibrium between matric potential and saturation is established, (ii) changes in saturation that occur when pressure is released and water flows from the ceramic plate back into the sample, (iii) redistribution of water into larger pores upon release of pressure, and (iv) long time period required to establish equilibrium between saturation and matric potential.

Specific details of the porous plate extractor methodology are as follows. A schematic for the pressure plate extractor apparatus is illustrated in Figure 3-3. The chamber was connected to an in-house compressed air source when testing at pressures below 6.89 bars (100 psi) and to an industrial grade nitrogen tank at higher pressures. The relative humidity of the pressurizing gas was increased to close to 100 percent relative humidity by placing a pool of water below the ceramic plate where it would not come into contact with the samples. Three porous ceramic plates, each with a different bubbling pressure (air-entry value), were used to determine the retention curves. The bubbling pressures of the plates were 2, 5, and 15 bars. The higher the bubbling pressure of the porous plate, the longer the time required for the saturation of the sample to come to equilibrium with a given gas pressure. Caution was taken to restrict the imposed gas pressure to less than the bubbling pressure of the ceramic plate, therefore ensuring that the ceramic plate remained saturated and that the gas would not pass through the plate.

The subsamples were initially saturated as defined in Section 3.1.2. The ceramic plates were saturated by repeatedly flushing them with deaired deionized water at pressures close to their bubbling pressure until bubbles ceased to be emitted. In order to ensure a good hydraulic connection between the subsamples and the ceramic plate, two precautions were exercised. First, the plate was lined with filter paper on which the subsamples were placed inside the pressure chamber. Next, a 227-g (8-oz.) lead weight was placed on top of each subsample.

The matric potential of the subsamples was measured by applying gas pressure into the chamber, which acted to force water out of the subsamples through the plate, the bottom of which was maintained at atmospheric pressure. After equilibrium was reached (after approximately 5 days) the partially saturated subsamples were removed from the chamber and weighed on a Mettler PM480 electronic balance to measure their mass. The subsamples were then returned to the chamber, which was again sealed and a greater pressure was applied. At the end of the test, the subsamples were dried in an oven at 105 °C until a constant weight was attained (usually 24 to 48 hr, depending upon the initial saturation level) to determine the dry weight of the sample. The matric potential at any point of the curve was thus equivalent to the pressure of the gas at that point. The percent saturation of the samples at a particular matric potential was calculated using the sample weight at that matric potential and the known saturated and dry weights by the following equation:

$$S = \frac{[\mathrm{wt}_{sat} - \mathrm{wt}_{read}]}{[\mathrm{wt}_{sat} - \mathrm{wt}_{dry}]} \times 100 \qquad (3\text{-}10)$$
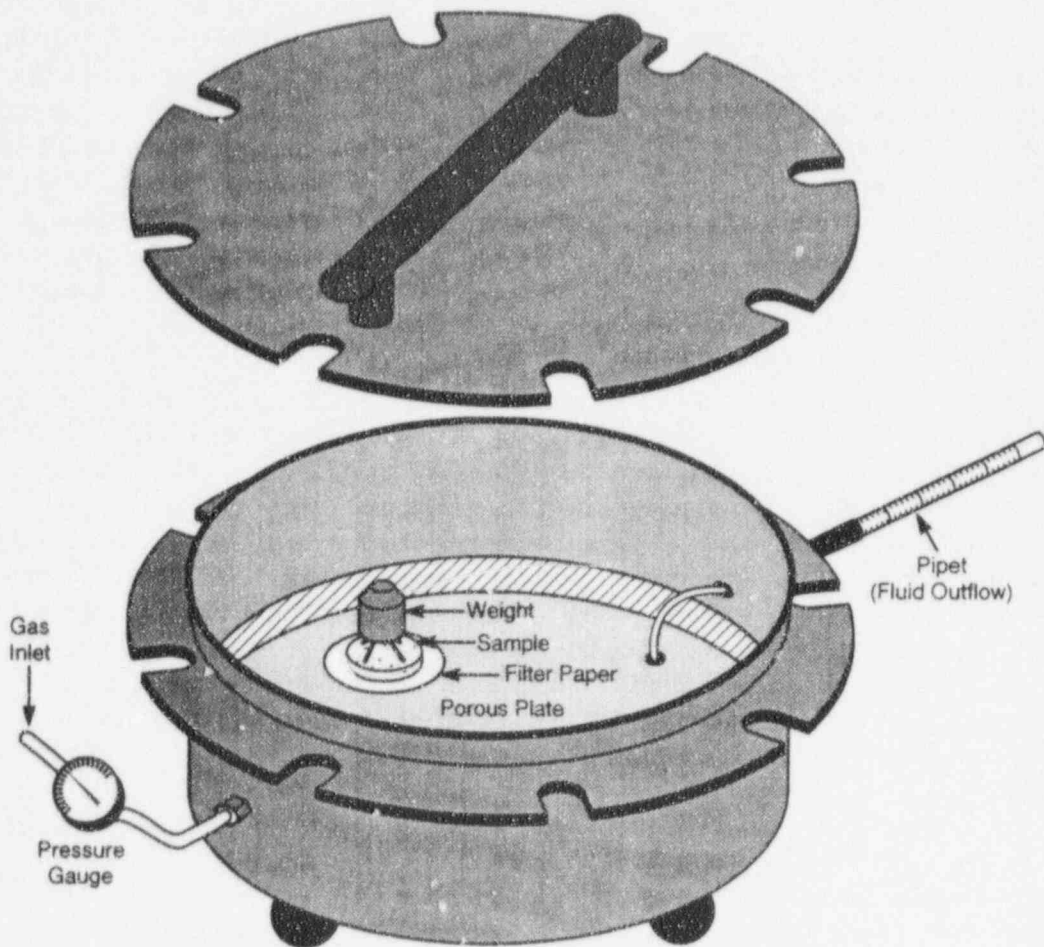
Figure 3-3. Schematic for a pressure plate extractor used to measure saturation/matric pressure relationships

where

S = sample percent saturation (-)

wt_{sat} = saturated sample weight (g)

wt_{read} = sample weight at a particular matric potential (g)

wt_{dry} = dry sample weight (g)

A total of 224 matric potential/saturation measurements was made using the pressure plate extractor method, with 34, 30, 14, 49, and 97 subsamples taken from NRG1, NRG2, NRG3, NRG4, and NRG5, respectively. The saturation/matric potential measurements made using the pressure plate extractor are listed in Appendix E.

3.2.2.2 Water Activity Meter

The matric potential/saturation relationship for subsamples at matric potentials greater than 10 bar were measured using an AquaLab CX2 water activity meter (Decagon Devices Inc.). The water activity meter measures matric potential by sensing the activity (A_w) of the water vapor, assumed to be in hydraulic equilibrium with the sample. Water vapor is measured by using a chilled mirror psychrometer located above a sample placed in a closed chamber (Gee et al., 1992).

A schematic of the AquaLab CX2 meter is illustrated in Figure 3-4. After placing a subsample in the chamber and engaging the instrument, a stainless mirror located above the sample in the chamber is repeatedly cooled and heated to form and drive off condensation. Each time condensation forms on the mirror, an infrared thermopile measures the temperature and activity (A_w) of the gas above the sample. When A_w values of consecutive readings are within 0.001, hydraulic equilibrium between the sample and the gas is assumed. Percent saturation of the subsamples was calculated using Eq. (3-9). The A_w was converted to matric potential function ψ by use of the Kelvin equation:

$$\psi = \frac{RT}{M} \ln (A_w) \qquad (3-11)$$

where

A_w = water activity coefficient (-)

T = temperature (K)

R/M = gas constant/molecular mass of water (4.61 mPa/k)

ψ = matric potential (Pa)

The matric potential/saturation relationship was determined using these measured water activity and saturation content values.

The small subsamples (A size) were used in the water activity measurements. A group of subsamples was initially saturated with deaired, deionized water as defined in Section 3.1.2. The weight of each saturated subsample was measured using a Mettler PM480 electronic balance, and sealed in a plastic sample cup with parafilm "M". At the beginning and end of each run, the AquaLab CX2 meter was checked for linear offset with prepared saturated salt standards. Saturated salt standards were selected to ensure that their A_w would bracket the A_w of the subsamples. Each subsample was initially weighed using a Mettler PM480 electronic balance, and then inserted into the activity meter. Upon completion of the A_w measurements, the A_w and temperature were recorded. The subsample was reweighed to account for any loss (gain) of moisture during the process. The subsamples were allowed to air dry to a new moisture content and then sealed with parafilm "M" in the sample cup. The subsamples were left sealed in the sample cup for up to 96 hr to allow the samples to come to uniform internal hydraulic equilibration, then the procedure was repeated. Both the time allowed for the subsample to attain internal equilibration and the time required to attain hydraulic equilibrium during measurement increased with decreasing moisture content..
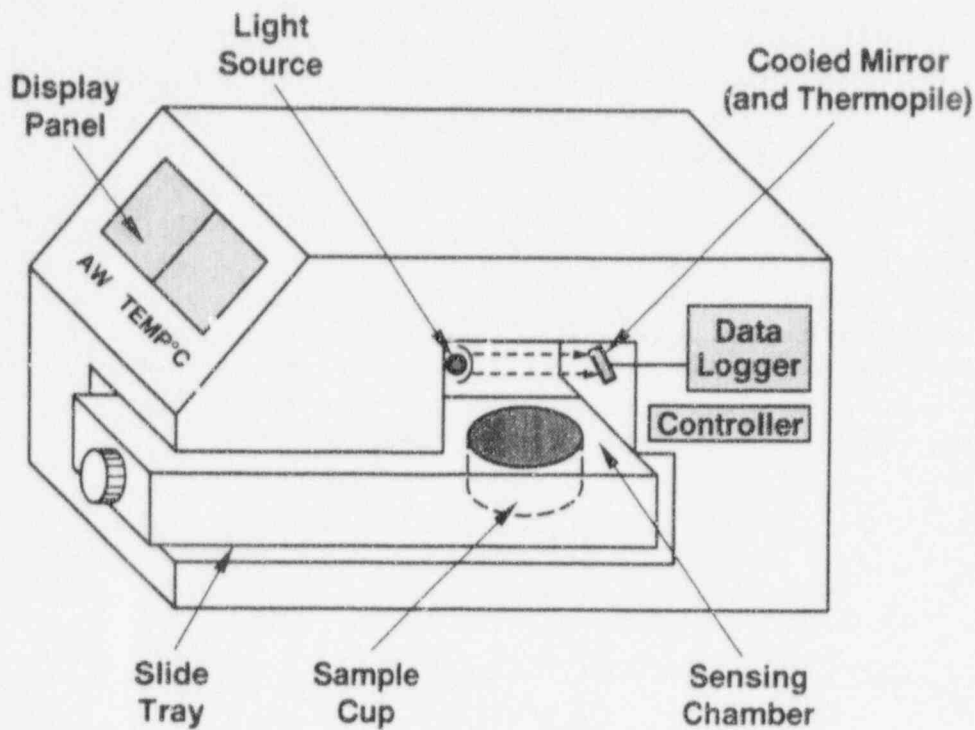
Figure 3-4. Schematic of an AquaLab CX2 water activity meter used to measure saturation/matric pressure relationships

The effective range of the activity meter was found to be from ~10 bar to over 1,000 bar matric potential. The documented accuracy of the AquaLab CX2 meter is 0.003 activity units, which equates to a matric pressure of ± 8 bar near full saturation and about ± 30 bar at the dry end of the retention curve. The meter was found to be sensitive to air movement in the laboratory and to ambient temperature changes. In order to minimize these effects, air vents in the testing area were closed and the meter was connected to a constant temperature water bath.

A total of 562 measurements was made using the AquaLab CX2 meter over a range of matric potentials/saturation to create moisture characteristic curves for the Nopal tuff samples. The matric potential/saturation measurements are listed in Appendix F.

4 RESULTS

Representative values for the matrix intrinsic properties and the matrix hydraulic properties have been determined for the five Nopal tuff samples. Parameter values and related statistics for the matrix intrinsic and hydraulic properties are presented in this section.

4.1 MATRIX INTRINSIC PROPERTIES

Measured values of bulk density, apparent specific gravity, bulk specific gravity, bulk specific gravity (SSD), and gravimetric and gas pycnometer porosities conducted on subsamples from the Nopal tuff samples are reported in this section. Included in the subsample statistics of the five Nopal tuff samples are the mean, coefficient of variation, minimum, median, and maximum values. The coefficient of variation is defined here as the standard deviation divided by the median.

4.1.1 Bulk Density

The mean, median, and coefficient of variation of the bulk density values have been calculated from the measured bulk density values for the subsamples from the five Nopal tuff samples. These statistics, in addition to the measured maximum and minimum values, are presented in Table 4-1. Overall, the value of bulk density increases with distance from the deposit from a low mean value of 1.847 g/cm^3 for NRG1 nearest the deposit to a maximum mean value of 2.374 g/cm^3 for NRG4, located farthest from the deposit. The skew of the data set is relatively small as evidenced by comparison of the mean and median values for each sample group. Within each sample group, little dispersion about the mean is evident in the relatively low values for the coefficient of variation. With the exception of NRG2, this dispersion increases with increasing bulk density.

4.1.2 Specific Gravity

The measured G_{app}, G_{bulk}, and G_{SSD} measurements for the five Nopal tuff samples are summarized in Tables 4-2, 4-3, and 4-4, respectively. The calculated mean, median, and coefficient of variation are also presented.

G_{app} measurements for the five Nopal tuff samples do not appear to vary relative to alteration in any discernible manner (Table 4-2). The mean of the five samples varies from a low of 2.495 to a high of 2.578. Variation within any one sample group is low, ranging from 0.007 to 0.039.

A summary of the G_{bulk} measurements and calculated statistics is presented in Table 4-3. In general, G_{bulk} decreases with increasing hydrothermal alteration. Mean values of the five Nopal tuff samples range from 1.899 near the deposit to 2.350 at a distance of about 400 m. The calculated variation of the measurements within each sample groups is low, ranging from 0.008 to 0.063.

G_{SSD} decreases near the deposit where hydrothermal alteration was at a maximum. Measurements of G_{SSD} (Table 4-4) are similar and slightly lower than those for G_{bulk}. The lower measurements may be attributable to buoyancy effects of isolated pores. Measurements of mean G_{SSD} vary from 2.161 to 2.413. Variation within each sample group is moderate, ranging from 0.017 to 1.997.

NUREG/CR-6356

Table 4-1. Bulk density of NRG1, NRG2, NRG5, NRG3, and NRG4 Nopal subsamples

Bulk Density (g/cm^3)					
Sample	NRG1	NRG2	NRG5	NRG3	NRG4
Mean	1.847	2.034	2.050	2.287	2.374
Coefficient of Variation	0.027	0.046	0.035	0.031	0.038
Minimum	1.652	1.885	1.858	2.076	2.140
Median	1.845	2.017	2.060	2.282	2.378
Maximum	1.976	2.230	2.217	2.457	2.587

Table 4-2. Apparent specific gravity, G_{app}, of NRG1, NRG2, NRG5, NRG3, and NRG4 Nopal tuff subsamples

Apparent Specific Gravity (G_{app})					
Sample	NRG1	NRG2	NRG5	NRG3	NRG4
Mean	2.574	2.578	2.515	2.495	2.571
Coefficient of Variation	0.008	0.007	0.039	0.037	0.037
Minimum	2.515	2.326	2.197	2.282	2.381
Median	2.575	2.562	2.534	2.478	2.562
Maximum	2.615	2.866	2.737	2.734	2.805

Table 4-3. Bulk specific gravity, G_{bulk}, of NRG1, NRG2, NRG5, NRG3, and NRG4 Nopal tuff subsamples

Bulk Specific Gravity (G_{bulk})					
Sample	NRG1	NRG2	NRG5	NRG3	NRG4
Mean	1.899	2.018	2.111	2.283	2.350
Coefficient of Variation	0.008	0.012	0.063	0.015	0.016
Minimum	1.870	1.962	2.033	2.140	2.260
Median	1.896	2.016	2.099	2.278	2.365
Maximum	1.937	2.087	2.880	2.363	2.403

Table 4-4. Bulk specific gravity saturated surface dry, G_{SSD}, of NRG1, NRG2, NRG5, NRG3, and NRG4 Nopal tuff subsamples

Bulk Specific Gravity (G_{SSD})					
Sample	NRG1	NRG2	NRG5	NRG3	NRG4
Mean	2.161	2.226	2.299	2.369	2.413
Coefficient of Variation	0.017	0.048	1.997	0.052	1.001
Minimum	2.132	2.168	2.237	2.309	1.627
Median	2.161	2.233	2.279	2.369	2.439
Maximum	2.187	2.264	3.140	2.422	2.460

4.1.3   Effective Porosity

Tables 4-5 and 4-6 present a summary of effective porosity measurements of the five Nopal tuff samples as measured by the gravimetric and gas pycnometer methods, respectively. Both measurement techniques indicate porosity increasing with increasing hydrothermal alteration toward the deposit. With the exception of NRG3, measured gas pycnometer porosity values are greater than gravimetric porosity values. Again, variation is small with a coefficient of variation ranging from 0.029 to 0.229 for the gravimetric method and 0.041 to 0.706 for the gas pycnometer method. The total range of porosity of the Nopal samples is large, from 0.036 to 0.270 as determined by the gravimetric method and from 0.02 to 0.34 percent as determined by the gas pycnometer method

4.2   MATRIX HYDRAULIC PROPERTIES

The hydraulic characterization methods described in Section 3.2 were used to measure the saturated hydraulic conductivity (K_{sat}) and the matric potential/saturation relationship of the five Nopal tuff samples. Additionally, unsaturated hydraulic conductivity was derived using the measured values for K_{sat} and the empirically determined relative permeability.

4.2.1   Saturated Hydraulic Conductivity

Saturated hydraulic conductivity values determined for the five Nopal tuff samples using the constant head permeameter method are summarized in Table 4-7. Flow rates at various pressure differentials were measured for each subsample. The relationships of pressure differential and flow rate for NRG1, NRG2, and NRG5 are linear except at large differential pressures, indicating that the flow through the subsamples was laminar only at low or moderate pressure differentials (i.e., where the relationship was linear). Hydraulic conductivity values that departed from the linear trend were determined to indicate either nonlaminar flow or some other unidentified inadequacy in the flow test. These nonlinear data were rejected from the sample statistics, and only those measurements in the linear range were used to calculate the saturated hydraulic conductivity for these three sample groups. Plots of hydraulic conductivity versus flow rate for subsamples from NRG3 and NRG4 did not exhibit linearity, and, in these cases, all measurements were included in the statistical calculations. This lack of linearity is attributed to difficulties in measuring saturated hydraulic conductivity for media with low conductivity. Figure 4-1 is a graph of flow rate versus pressure differential for the complete set of subsamples tested. Included in this graph are all linear data for samples NRG1, NRG2, NRG5 and all data, irrespective of linearity, for samples NRG3 and NRG4. Plots of individual results are included in Appendix E. Hydraulic conductivity measurements for the five Nopal tuff samples varied by over four orders of magnitude (i.e., 6.22×10^{-14} to 1.5×10^{-9} m/s).

4.2.2   Retention Curve

Composite data from the measurement of the matric pressure/saturation relationship have been graphically presented as retention curves for samples NRG1 through NRG5 in Figures 4-2 through 4-6. An empirical relationship was fit to the data set for each rock sample using the computer program RETC (van Genuchten et al., 1991). The empirical form of the matric pressure/saturation potential relationship is taken from van Genuchten (1980)

Table 4-5. Gravimetric porosity of NRG1, NRG2, NRG5, NRG3, and NRG4 Nopal tuff subsamples

Porosity (Gravimetric)					
Sample	NRG1	NRG2	NRG5	NRG3	NRG4
Mean	0.255	0.210	0.183	0.083	0.078
Coefficient of Variation	0.029	0.061	0.060	0.229	0.149
Minimum	0.235	0.169	0.154	0.036	0.053
Median	0.256	0.213	0.188	0.089	0.074
Maximum	0.270	0.226	0.021	0.126	0.113

Table 4-6. Pycnometric porosity of NRG1, NRG2, NRG5, NRG3, and NRG4 Nopal tuff subsamples

Porosity (Gas Pycnometric)					
Sample	NRG1	NRG2	NRG5	NRG3	NRG4
Mean	0.30	0.26	0.21	0.08	0.13
Coefficient of Variation	0.04	0.12	0.12	0.71	0.55
Minimum	0.28	0.23	0.18	0.02	0.04
Median	0.29	0.25	0.20	0.06	0.12
Maximum	0.32	0.34	0.26	0.18	0.31

Table 4-7. Saturated hydraulic conductivity of NRG1, NRG2, NRG5, NRG3, and NRG4 Nopal tuff subsamples

Saturated Hydraulic Conductivity (m/s)					
Sample	NRG1	NRG2	NRG5	NRG3	NRG4
Mean	9.49×10^{-10}	4.09×10^{-10}	1.95×10^{-10}	1.09×10^{-12}	2.17×10^{-12}
Coefficient of Variation	0.556	0.191	0.509	0.995	0.312
Minimum	1.15×10^{-10}	2.78×10^{-10}	9.67×10^{-11}	6.22×10^{-14}	1.17×10^{-12}
Median	1.06×10^{-9}	4.23×10^{-10}	1.91×10^{-10}	7.97×10^{-13}	2.42×10^{-12}
Maximum	1.5×10^{-9}	5.19×10^{-10}	3.67×10^{-10}	2.20×10^{-12}	2.65×10^{-12}

$$S_e = \frac{1}{[1 + (\alpha h)^n]^m} \tag{4-1}$$

where S_e is the effective saturation, h is the hydraulic head (m), and α, n, and m are fitting parameters that affect the shape of the retention curve. The α parameter is related to the inverse of the air-entry or bubbling pressure of the medium, expressed in m^{-1} of water. Equation (4-1) is commonly referred to as the van Genuchten retention equation. Effective saturation can be defined as

$$S_e = \frac{\theta - \theta_r}{\theta_s - \theta_r} \tag{4-2}$$

where θ is volumetric water content and the r and s subscripts refer to residual and saturated states, respectively.

A closed-form solution for relative liquid permeability can be formulated by incorporating the van Genuchten retention equation into an analytical solution relating hydraulic head, saturation, and permeability (Mualem, 1976) to provide a definition for relative liquid permeability, k_{rl}, as follows (Nitao, 1988)

$$k_{rl} = \frac{[1 - (\alpha h)^{n-1} [1 + (\alpha h)^n]^{-m}]^2}{[1 + (\alpha h)^n]^{\frac{m}{2}}} \tag{4-3}$$

Liquid relative permeability is expressed in terms of head and the three fitting parameters, α, n, and m. The number of fitting parameters in Eqs. (4-2) and (4-3) can be reduced from three to two by assuming

$m=1-1/n$, a relationship frequently invoked with many classes of geologic material especially when the amount of retention data is limited (van Genuchten et al., 1991). The two resulting fitting parameters, α and n, are referred to as the van Genuchten parameters.

A van Genuchten retention curve has been fit to all five sets of measured retention data. Although the RETC code provides for an inverse solution to fitting a curve to retention curve data, only trial and error forward solution curve fits were used in these analyses. The inverse solutions were inadequate, possibly due to inappropriate weighting in the least squares routine caused by the inordinate amount of data available at low saturation levels. The resulting retention curves have been graphically presented with the retention data in Figures 4-2 through 4-6. As illustrated, van Genuchten retention curves provide reasonable approximations for the retention data. Values for the van Genuchten α and n parameters for these five fitted curves are presented in Table 4-8. The van Genuchten retention curves for the five Nopal samples are plotted in Figure 4-7 for comparison. Two general observations of the relationships among the curves can be made. First, the air-entry values for all five samples are similar. The air-entry value can be defined as the suction pressure required to de-water the largest set of pore volumes present in a porous medium. This relationship is contrary to findings by Wang (1992), in which a discernible relationship between permeability and the α parameter was observed among tuffs from YM and the Apache Leap site and soils from the Las Cruces trench. The similarity in air-entry values for the Nopal samples is attributed to two possible sources: (i) relatively no change in the size of the largest pores even though the pore-size distribution was changed by hydrothermal alteration activities or (ii) a lack of accuracy in matric pressure/saturation relationship measurements at high-saturation values, possibly related to the practice of saturating samples to 100 percent, which may be in excess of full saturation values observed in the field. Regardless of the source of the apparent similarity, the total range of the calculated air-entry values is from 5 bars (equivalent to a van Genuchten α value of 0.2 bars^{-1}) to 10 bars (equivalent to a van Genuchten α value of 0.1 bar^{-1}).

Table 4-8. Van Genuchten α and n parameters for NRG1, NRG2, NRG5, NRG3, and NRG4 Nopal tuff subsamples

Sample	NRG1	NRG2	NRG5	NRG3	NRG4
α (m^{-1})	0.12	0.175	0.1	0.20	0.20
n	2.00	1.60	1.80	1.35	1.30

The second observation apparent in the relationships among the retention curves is that the slope of the retention curve increases with a decrease in the saturated hydraulic conductivity. Note that large van Genuchten n values equate with low retention curve slopes, an indication of narrow pore-size distributions. Sample NRG1, with the largest degree of alteration and the greatest saturated hydraulic conductivity at 1.06×10^{-9} m/s, has the largest calculated value for the van Genuchten n parameter at 2.0. Samples NRG3 and NRG4, which resemble the unaltered host rock, have saturated hydraulic conductivities of 2.42×10^{-13} and 7.97×10^{-12} m/s and van Genuchten n values of 1.35 and 1.30, respectively.
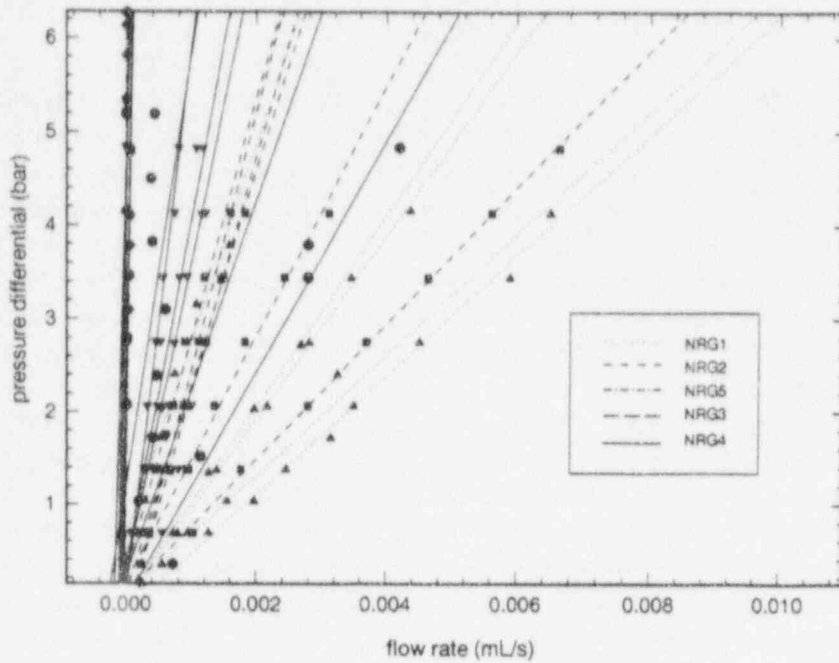
Figure 4-1. Flow rate (mL/s) plotted versus pressure differential (bar) measurements from constant head permeability experiments for Nopal samples
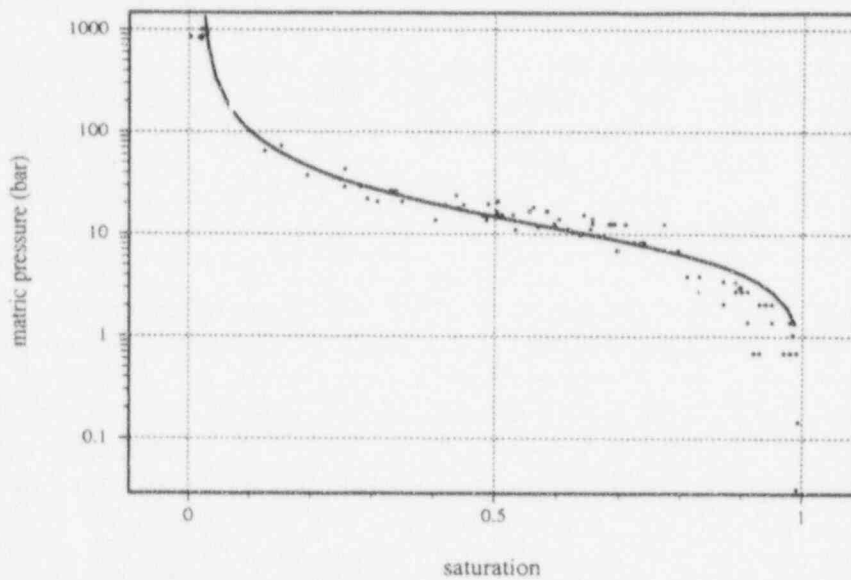
Figure 4-2. Moisture retention data and fitted curve for NRG1. Van Genuchten α and n parameters have values of 0.12 m^{-1} and 2.0, respectively.
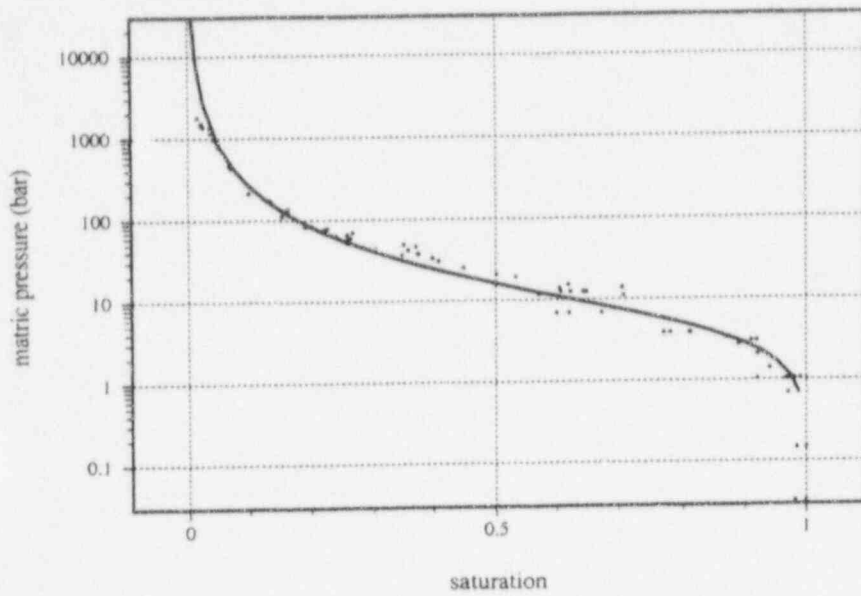
Figure 4-3. Moisture retention data and fitted curve for NRG2. Van Genuchten α and n parameters have values of 0.175 m^{-1} and 1.6, respectively.
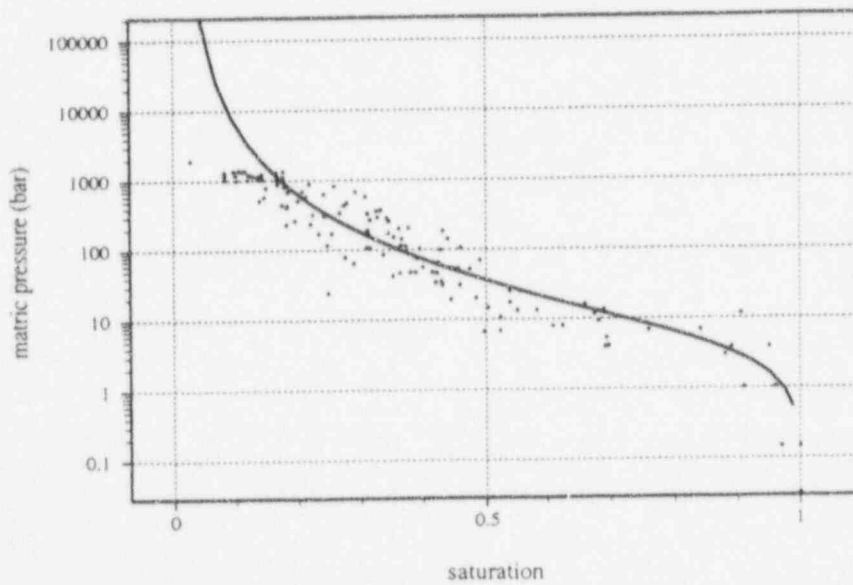
Figure 4-4. Moisture retention data and fitted curve for NRG3. Van Genuchten α and n parameters have values of 0.20 m^{-1} and 1.35, respectively.
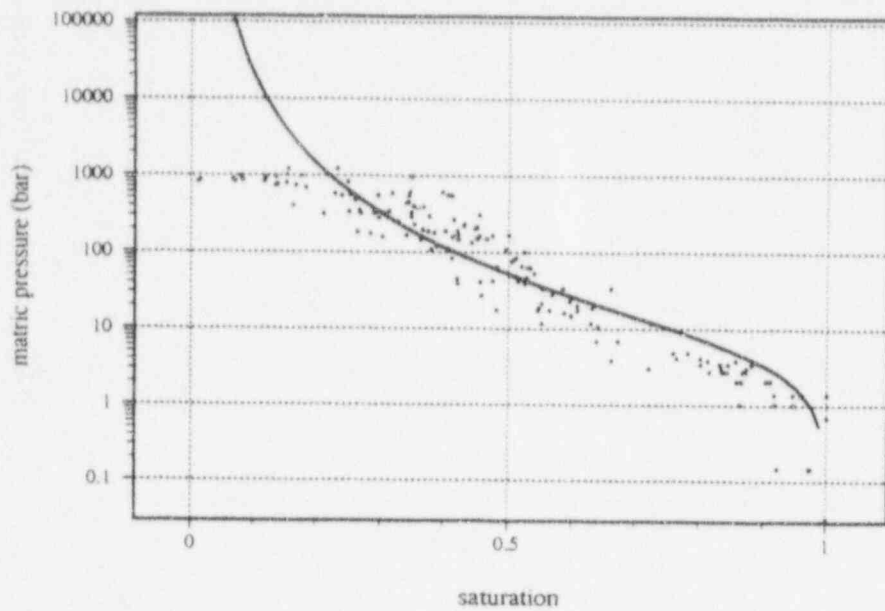
Figure 4-5. Moisture retention data and fitted curve for NRG4. Van Genuchten α and n parameters have values of 0.20 m^{-1} and 1.30, respectively.
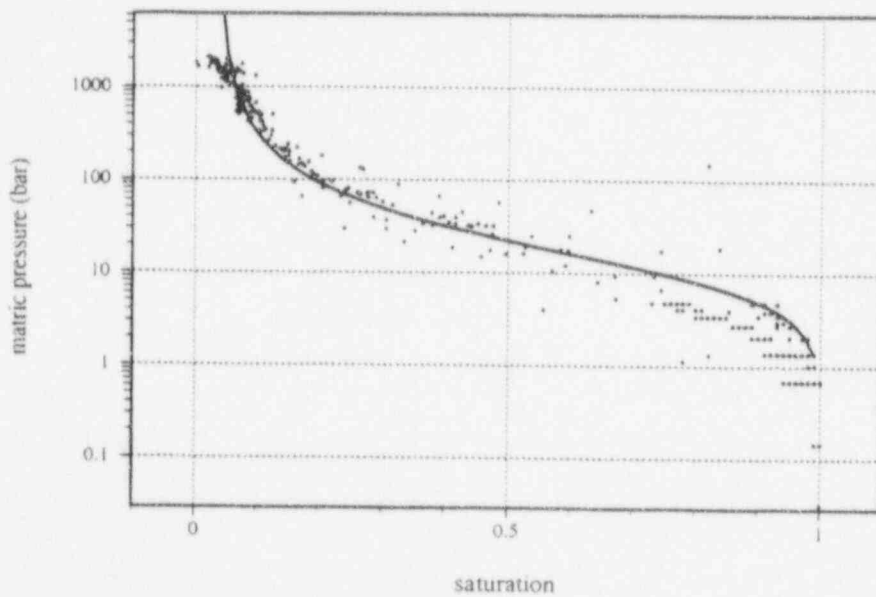
Figure 4-6. Moisture retention data and fitted curve for NRG5. Van Genuchten α and n parameters have values of 0.10 m^{-1} and 1.80, respectively.
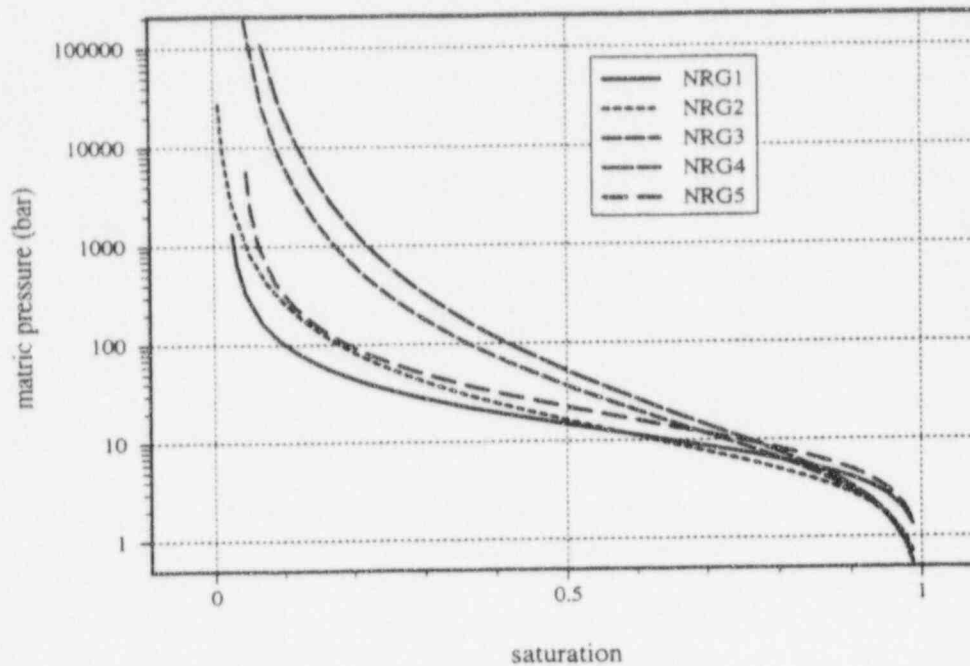
Figure 4-7. Fitted van Genuchten curves for NRG1, NRG2, NRG3, NRG4, and NRG5 Nopal tuff samples

The relationship between the saturated hydraulic conductivity and the slope of the retention curve (more exactly, the van Genuchten n parameter) for the samples collected at Nopal has been evaluated. The log of the measured saturated hydraulic conductivity values for the five Nopal samples has been plotted relative to the calculated van Genuchten n parameter in Figure 4-8. Error bars have been included to illustrate the range in measured hydraulic conductivity values for each of the Nopal samples. In general, the value of the van Genuchten n parameter increases linearly as the log of the median saturated hydraulic conductivity decreases. The linear relationship between the van Genuchten n parameter and log of the median of the saturated hydraulic conductivity has been identified in the graph. This least-squares linear fit to the data has the following form

$$\log K_{sat} = 4.2n - 14.9 \tag{4-4}$$

This relationship can be expressed in terms of K_{sat} (with minor approximation of its coefficients) as

$$K_{sat} = 10^{(4n-15)} \tag{4-5}$$

This general relationship provides a means to approximate the van Genuchten n parameter at the Nopal site when the saturated hydraulic conductivity is known. An analogous relationship between saturated hydraulic conductivity and the van Genuchten α parameter has not been identified, ostensibly

since measured values for α were relatively constant in all samples collected and tested from the Nopal site. Using the observation that the van Genuchten α parameter is constant and that the van Genuchten n parameter can be calculated from K_{sat} allows characterization of the unsaturated hydraulic properties of media at locations at the site other than those fully tested. Use of this relationship would aid in site characterization since saturated hydraulic conductivity is significantly easier to determine than the retention curve.

4.2.3 Unsaturated Hydraulic Conductivity

Unsaturated hydraulic conductivity for the five rock samples was calculated as the product of the measured saturated hydraulic conductivity and empirically determined liquid relative permeability as follows

$$K(\psi) = k_{rl} K_{sat} \qquad (4\text{-}6)$$

Unsaturated hydraulic conductivity for the five samples has been calculated using the measured values for saturated hydraulic conductivity and the value for the liquid relative permeability defined in Eq. (4-3) and determined using retention curves fit to the measured retention data. These values are graphically illustrated as a function of matric potential in Figure 4-9.
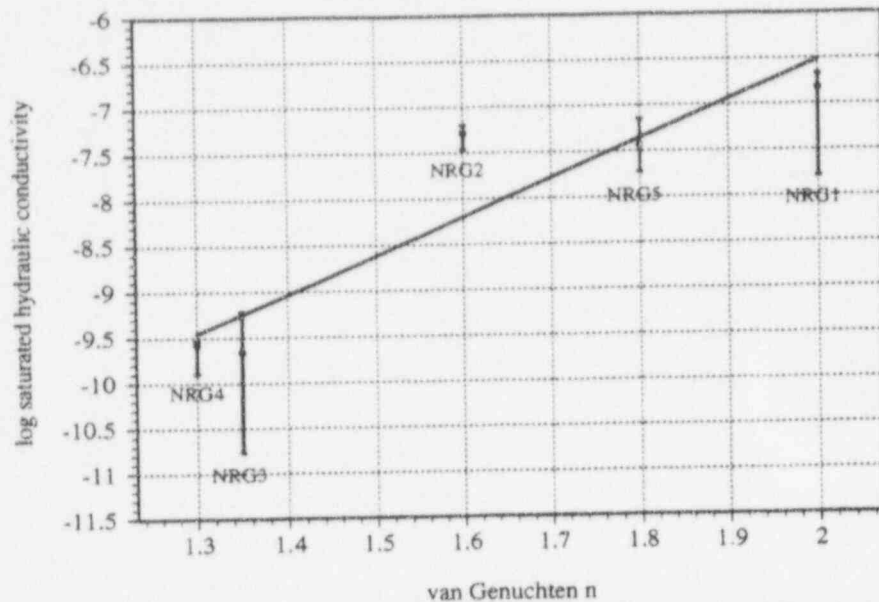
Figure 4-8. Correlation of log saturated hydraulic conductivity (cm/s) and the van Genuchten *n* parameter. Error bars indicate the range in measured saturated hydraulic conductivity values. The line is a least-square regression of the median values of the log saturation hydraulic conductivity.
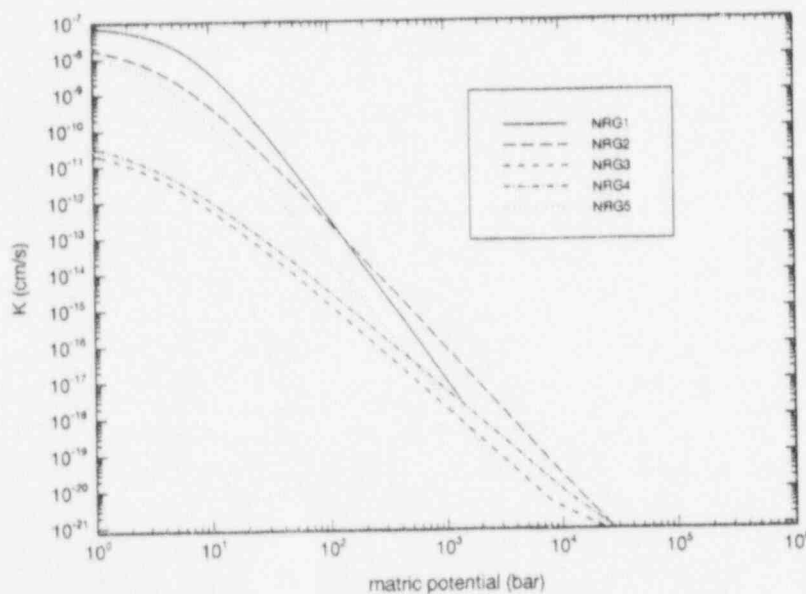
Figure 4-9. Unsaturated hydraulic conductivity calculated using measured saturated hydraulic conductivities, van Genuchten retention curve parameters, and the van Genuchten-Mualem closed-form solution

4-13

5 PERCOLATION SIMULATION EVALUATION

Analyses of water percolating through partially saturated, fractured tuff were conducted as part of the integrated effort with the Natural Analog Research Project to investigate flow and transport through fractured-porous media. In further support of this integrated effort, a proposed percolation tracer experiment at the Peña Blanca natural analog site has been identified to assist in evaluating conceptual and mathematical models for flow and transport through partially saturated, fractured tuff. Percolation at the Peña Blanca site has been simulated to assess the feasibility of proposed field experiments. The fortuitous geometric and physical attributes of the Peña Blanca natural analog qualify the site for such an experiment. These attributes include an extensive area of exposed rock (identified as the +10 level), a series of existing 4-in. (10.2-cm) diameter boreholes, and 80 m of adit associated with previous mining activities (Pearcy et al., 1993). The proposed field-scale percolation test entails infiltrating water from the +10 level and monitoring the arrival of the water in the adit located at a depth of 8 to 10 m. This field test provides the opportunity to observe the arrival of water with conservative or nonconservative tracers after moving through 8 to 15 m of partially saturated, fractured tuff. In addition, the location of a brecciated U zone at the analog site provides a system with a range of physical and hydraulic properties (i.e., porosity, hydraulic conductivity, unsaturated flow parameters, and fracture characteristics) that permit the examination of flow and transport through a variety of physical systems relevant to and expected to be present at YM.

The proposed field experiment is designed to test conceptual and mathematical models of percolation processes expected below the horizon where infiltration is significant. Models for near-surface infiltration will not be tested because the surface at the analog site at Peña Blanca has been altered (i.e., surface sediments, vegetation, and weathered rock have been removed) to reduce most of the near-surface processes that affect infiltrating water. The conceptual model of the proposed field-scale percolation test specifies that water is introduced into the subsurface along a 3-m wide zone directly over the long dimension of the adit. A series of conceptual models of the fractured tuff at the Peña Blanca natural analog site is assessed in this analysis, the first characterizing the medium as a uniform, homogeneous porous medium, and the remainder characterizing the medium as a homogeneous composite of fractures and rock matrix (Wang and Narasimhan, 1986; Klavetter and Peters, 1986; Nitao, 1988). Additionally, the effects of different assumed aperture sizes were evaluated. Inherent in the composite conceptual model is an assumption of hydraulic equilibrium between water present in the matrix and in the fractures. Evaluation of a nonequilibrium relationship between matrix and fracture water requires a different conceptual model. Only the composite model described by Klavetter and Peters will be assessed in this evaluation. Flow of groundwater for the conceptual models was simulated with an adapted version of the numerical code V-TOUGH (Pruess, 1987 and Nitao, 1989), and the results are compared. The adapted version, C-TOUGH, differs from V-TOUGH in that it has an iterative solver and modified data input and output subroutines.

5.1   MODEL DEVELOPMENT

A vertical two-dimensional (2D) numerical flow model was assembled to replicate the subsurface at the Peña Blanca natural analog site. A 2D characterization is assumed adequate, particularly during the preliminary phases of these analyses, as water can be infiltrated along a strip source directly overlying the adit. The model assumes symmetry through the vertical axis of the adit and extends from the surface to a depth of 12 m in the z-direction and from the vertical axis of the 3-m wide adit to a distance of 12 m in the x-direction (Figure 5-1). Infiltration of water through the modeled medium is simulated by
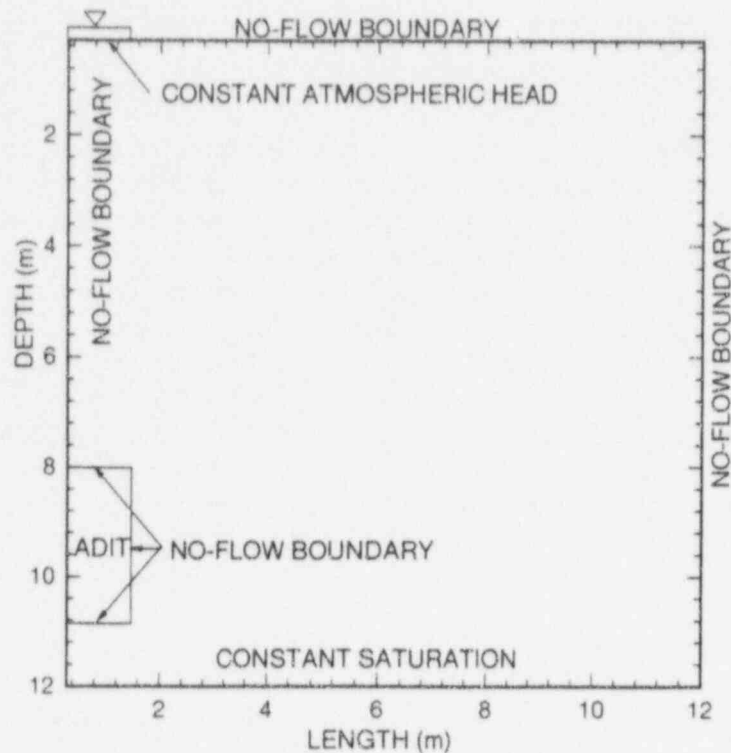
Figure 5-1. Schematic of infiltration model for Peña Blanca

establishing the hydraulic head at atmospheric pressure over a 1.5-m wide section (equal to a 3-m wide section for the entire cross section of the adit) along the upper boundary of the model directly over the adit. The model contains 40 equally spaced rectilinear elements in both the vertical and horizontal coordinate directions. The vertical and top boundaries are no-flow boundaries (with the exception of the 1.5-m wide infiltration section). The bottom boundary is established at a constant saturation of 0.5, the same as the initial saturation of the interior nodes. The constant saturation condition at the base is considered adequate for early time simulations but loses validity as the wetting front nears the bottom of the domain.

The adit has a height and total width of 3 m and is established as an extremely low-permeability zone as a preliminary characterization of a seepage face. This coarse characterization of the adit boundary is equivalent to a no-flow boundary at the adit wall. The adit boundary treatment is considered adequate because liquid flow regime above the adit and the approximate arrival time of the infiltration front at the adit boundary, rather than quantification of water seeping into the adit, are of interest at this time.

The permeability and retention curve parameters assigned to the matrix in the simulations were determined from property values measured in the laboratory on the variably altered rocks sampled from the Nopal Formation at Peña Blanca. The attributes of fractures at the Nopal site have not been directly measured. Appropriate use of ancillary information of the fractures, however, permits fracture property estimates to contain less uncertainty as compared to standard values taken from the literature. Fracture

information from Nopal includes the mapping of over 11,000 fractures (Pearcy, 1994). Fracture density has been determined using this mapping. Preliminary characterization of fractures has been performed, although final assignment of fracture properties has not yet been attempted, and fracture aperture measurements are not yet available. Fractures mapped by Pearcy include those discernible at a height of about 2 m. This mapping precludes microfractures. This measurement threshold appears sufficient for this analysis since microfractures at the Nopal site are interpreted to have apertures of less than about 1 μm, an aperture assumed not to significantly contribute to fluid flow. An average aperture estimate of 100 μm appears reasonable for the Nopal[1]. Analysis of the effect of average apertures one order of magnitude greater than or less than 100 μm provides a measure of the sensitivity of percolation rates to fracture aperture.

Fracture porosity values for the Nopal site were determined by multiplying measured surficial fracture density measurements with the estimated average fracture apertures. Fracture porosities of 2×10^{-5}, 2×10^{-4}, and 2×10^{-3} are calculated using an average fracture density of 2 m/m^2 measured at the Nopal site (Pearcy, 1994) and estimated average fracture apertures of 10, 100, and 1,000 μm. Fracture permeability was calculated using the cubic law (Snow, 1968; Schwartz and Domenico, 1990)

$$K_f = \frac{Nb^3}{12} \qquad (5\text{-}1)$$

where N is the length of fractures per unit area and b is the aperture. Fracture permeabilities calculated for each of the three assumed average apertures are 1.7×10^{-16}, 1.7×10^{-13}, and 1.7×10^{-10} m^2, respectively. Fracture hydraulic conductivity, K_f, was again calculated using the cubic law (Snow, 1968; Schwartz and Domenico, 1990)

$$K_f = \frac{\rho Nb^3}{12\mu} \qquad (5\text{-}2)$$

where μ is viscosity and ρ is the density of water. Fracture hydraulic conductivities for estimated average fracture apertures of 10, 100, and 1,000 μm are 8.2×10^{-10}, 8.2×10^{-7}, and 8.2×10^{-4} m/s, respectively. Fracture porosity, permeability, and hydraulic conductivity for each assumed average fractured aperture are summarized in Table 5-1. The fracture unsaturated hydraulic characteristics for media at Nopal have not been measured. Assigned values for the van Genuchten parameters were taken from Klavetter and Peters (1986). Accordingly, a value of 4.23 has been assigned to n and 1.2851 m^{-1} has been assigned to α. The relative permeability for the equivalent continuum model can be expressed as a volume average of the fracture and matrix relative permeabilities (Wang and Narasimhan, 1986; Klavetter and Peters, 1986; Nitao, 1988)

$$k_{rl}^B = \frac{[K_f k_{rl}\phi_f + K_m k_{rl}^m (1 - \phi_f)]}{K_B} \qquad (5\text{-}3)$$

---

1. E.C. Pearcy, personal communication.

Table 5-1. Calculated fracture characteristics

Fracture Aperture (μm)	Fracture Porosity	Fracture Permeability (m²)	Fracture Hydraulic Conductivity (m/s)
10	2×10^{-5}	1.7×10^{-16}	8.2×10^{-10}
100	2×10^{-4}	1.7×10^{-13}	8.2×10^{-7}
1,000	2×10^{-3}	1.7×10^{-10}	8.2×10^{-4}

where the B, f, and m subscripts refer to the bulk, fracture, and matrix, respectively, ϕ is porosity, and the saturated bulk liquid hydraulic conductivity, K_B, is defined by

$$K_B = K_f \phi_f + K_m (1 - \phi_f) \qquad (5-4)$$

Bulk permeability was calculated using Eqs. (5-3) and (5-4) for each combination of measured matrix hydraulic property sets (i.e., NRG1, NRG2, etc.) and assumed fracture properties. Calculated bulk permeability values for the 15 matrix/fracture combinations and for assumed fracture apertures of 1, 10, 100, and 1,000 μm are summarized in Table 5-2. Bulk permeability values for an aperture of 1 μm are included here to compare the relative contribution to flow by 1 and 10 μm aperture fractures.

Table 5-2. Bulk permeability k_b (m²) of NRG1, NRG2, NRG5, NRG3 and NRG4 Nopal tuff subsamples

Fracture Aperture (μm)	NRG1	NRG2	NRG5	NRG3	NRG4
1	1.06×10^{-16}	4.31×10^{-17}	1.95×10^{-17}	8.13×10^{-20}	2.47×10^{-19}
10	1.06×10^{-16}	4.31×10^{-17}	1.95×10^{-17}	8.46×10^{-20}	2.50×10^{-19}
100	1.39×10^{-16}	7.65×10^{-17}	5.29×10^{-17}	3.35×10^{-17}	3.36×10^{-17}
1,000	3.34×10^{-13}	3.34×10^{-13}	3.34×10^{-13}	3.34×10^{-13}	3.34×10^{-13}

5.1.1 Numerical Simulations

Simulation results of water percolating through fractured porous media were evaluated to compare arrival times of water at the adit and the nature of the water front advancing through the subsurface. Because the hydraulic boundary at the adit wall was represented as a no-flow boundary for simplicity and not as a seepage face, percolating water was not correctly modeled when it encountered the adit. Therefore, simulation predictions at the time when the 0.60 saturation contour neared (i.e., within about 1.0 m) the upper boundary of the adit were identified in these evaluations as the arrival time of water

at the adit. This approximation appears to be sufficient for the purposes of this comparative evaluation of percolation models. Saturation contour plots at the time when the 0.60 saturation contour is near the adit's upper boundary are presented in Figures 5-2 through 5-6 for the five sample rock types, all with an assigned average fracture aperture of 10 μm. As illustrated in these simulation results, the time required for the water front (as indicated by the 0.60 saturation contour) to arrive at the adit varies from about 25 yr for the most conductive sample, NRG1, to as long as 10,000 yr for the unaltered NRG3 and NRG4 samples. As illustrated by the calculated bulk permeability value in Table 5-2, the contribution to percolation of water by fracture flow is negligible for fractures with apertures of 10 μm or less. An exception to the statement is in the case of NRG3, with the lowest measured matrix hydraulic conductivity at 7.97×10^{-13} m/s, in which a slight increase in flow by 10-μm fractures was observed. This observation was supported by noting that simulations of percolation for the five media types with average apertures of 1 μm (not shown here) were essentially identical to predictions with average fracture apertures of 10 μm. Predictions of flow with assumed average fracture apertures of 1 and 10 μm, therefore, are analogous to matrix flow only conceptual models. In simulations with an average fracture aperture not exceeding 10 μm, flow was controlled by the matrix. In this matrix-dominated flow (i.e., composite models), the advancing wetting fronts are diffuse with no indication of a sharp saturation gradient.

Figures 5-7 through 5-11 illustrate saturation contours for simulations assuming average fracture apertures of 100 μm. The wetting front saturation contours are plotted at times in which the 0.60 contours are again near the upper adit boundary. In these cases, simulation results for all five media types exhibited arrival times shorter than arrival times in comparable media with matrix flow only, particularly in the simulations of the NRG3 and NRG4 media whose matrices have the lowest hydraulic conductivities. Distinct differences are apparent between the wetting front patterns of these two media and the wetting front patterns of NRG1, NRG2, and NRG3, all of which exhibit hydraulic conductivities almost two orders of magnitude greater than those for the matrices of NRG3 and NRG4. A much sharper and more rapid wetting front is observed in NRG3 and NRG4 than in any of the other three media. Arrival time of the 0.60 saturation contour at the adit boundary is about 20 yr for the low-conductivity media compared to about 50 yr for the highly conductive media. This discrepancy is not directly attributed to differences in hydraulic conductivity. This difference in arrival time is attributed instead to the large difference in matrix porosity (0.20 to 0.29 in the high conductivity media and 0.06 to 0.12 in the low-conductivity media) and the assumption of matrix/fracture hydraulic equilibrium inherent in the composite conceptual model. This assumption of hydraulic equilibrium can lead to inaccurate predictions, particularly in media with significant porosities. In composite models, the equilibrium assumption requires that both matrix and fracture components of the continuum are maintained at the same hydraulic potential at all times, including the time during which the wetting front advances through the medium. Percolating water cannot advance through fractures in the numerical model at a rate in excess of the rate at which water is made available to the entire matrix of a numerical element. Sufficient water has to be imbibed by the matrix to bring it to hydraulic equilibrium with the element fractures prior to fracture flow out of the element. This requirement, coupled with the physics of capillarity which dictate that the matrix will be essentially fully saturated prior to flow through fractures that are considered large (i.e., 100 μm or greater), prohibits fracture flow except in regions where the matrix is essentially saturated.

Figures 5-12 through 5-16 illustrate saturation contours for simulations assuming average fracture apertures of 1,000 μm at times in which the 0.60 contours are again near the upper adit boundary. In all simulations with an assigned fracture aperture of 1,000 μm, an abrupt wetting front is predicted. Similar to simulations of flow with an assumed fracture aperture of 100 μm, arrival times in simulations of media with large porosities are greater than arrival times for media with low porosity irrespective of matrix

Figure 5-2. Wetting front at 18 yr for 10-μm fractures in NRG1

Figure 5-3. Wetting front at 70 yr for 10-μm fractures in NRG2

Figure 5-4. Wetting front at 10,000 yr for 10-μm fractures in NRG3

Figure 5-5. Wetting front at 9,000 yr for 10-μm fractures in NRG4

5-7
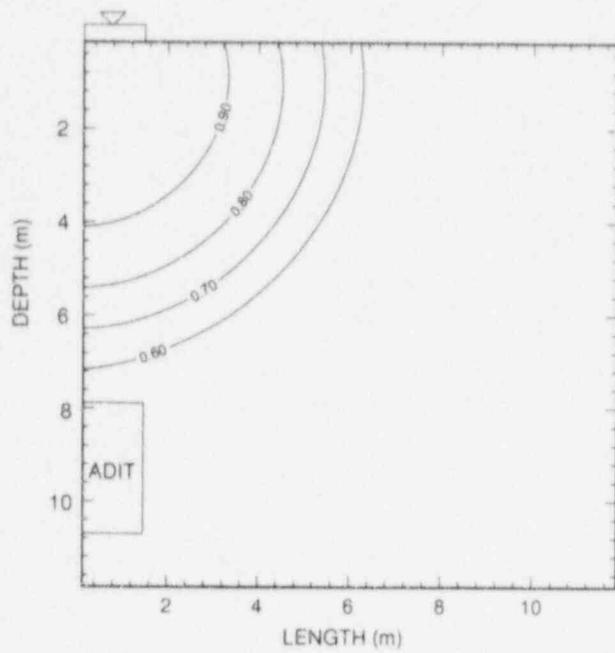
Figure 5-6. Wetting front at 70 yr for 10-μm fractures in NRG5
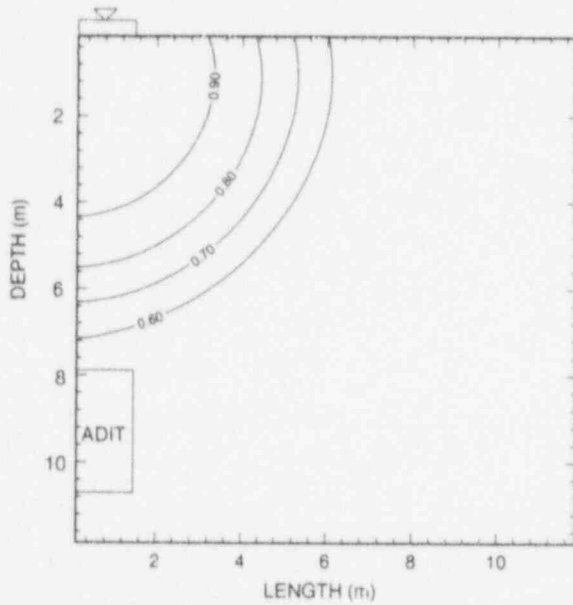
Figure 5-7. Wetting front at 20 yr for 100-μm fractures in NRG1

5-8
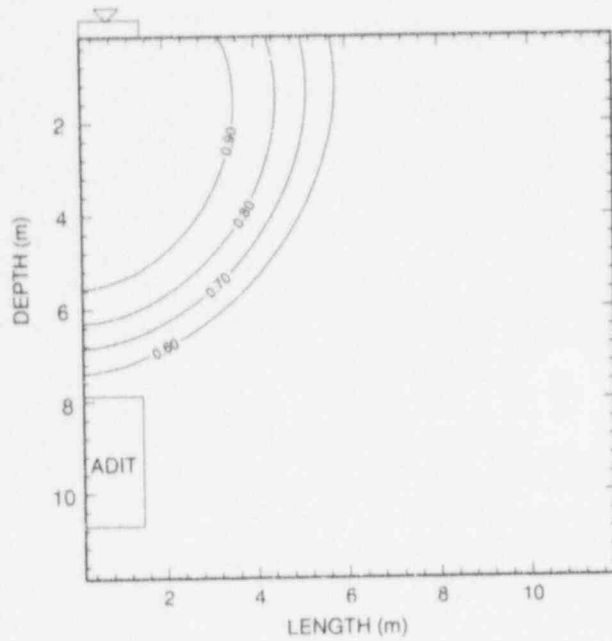
Figure 5-8. Wetting front at 50 yr for 100-μm
fractures in NRG2

Figure 5-9. Wetting front at 20 yr for 100-μm
fractures in NRG3

5-9
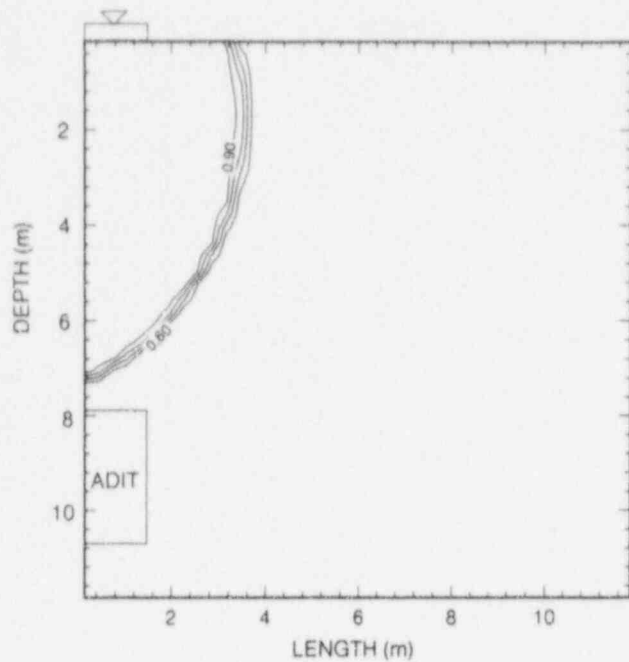
Figure 5-10. Wetting front at 45 yr for 100-μm fractures in NRG4
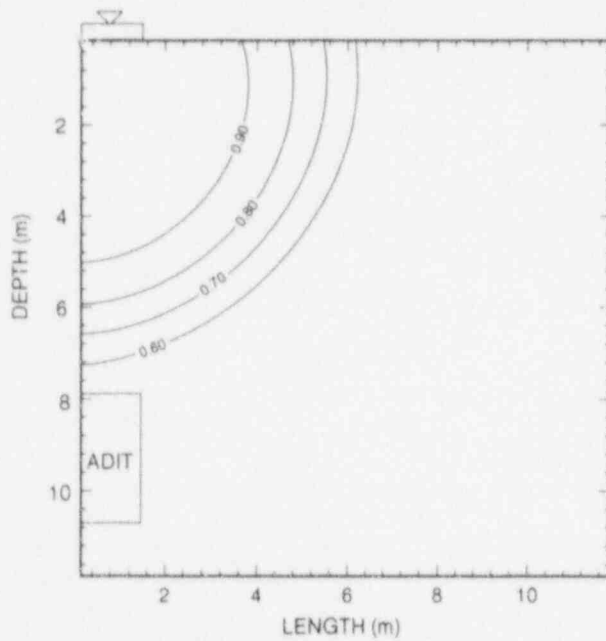
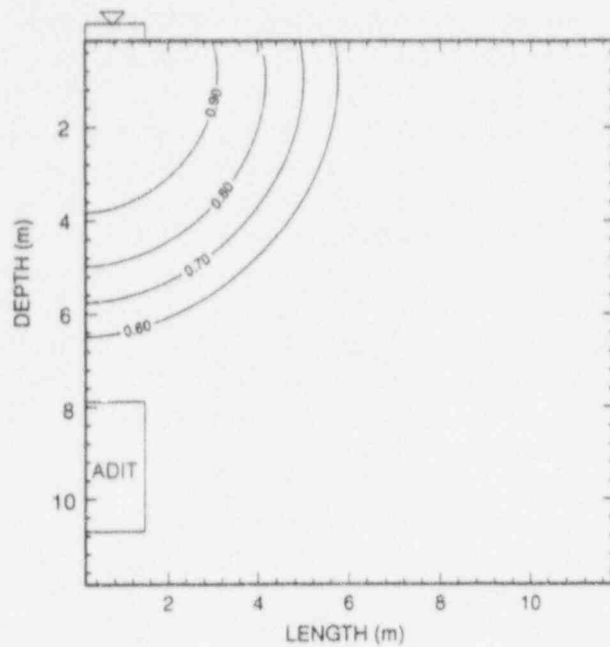**Figure 5-11.** Wetting front at 50 yr for 100-μm fractures in NRG5

5-10
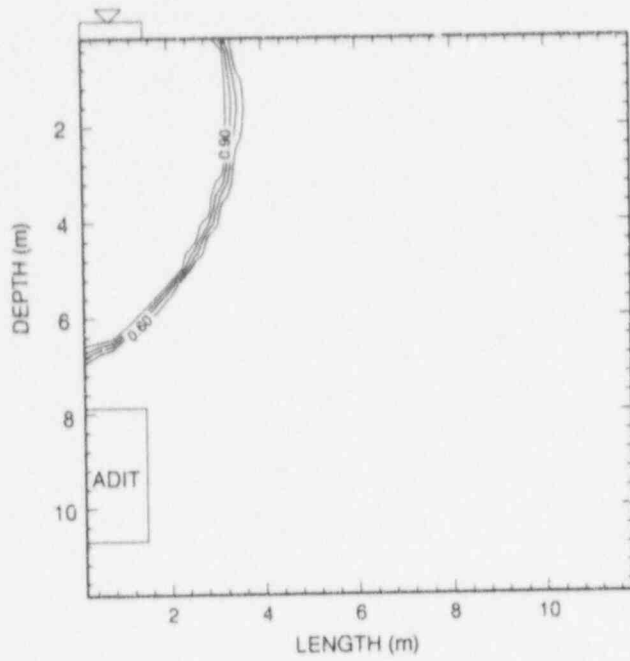
Figure 5-12. Wetting front at 0.01 yr for 1,000-μm
fractures in NRG1
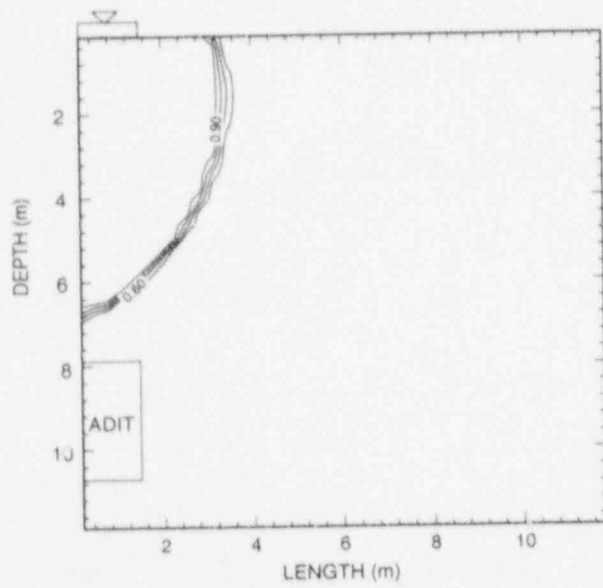
Figure 5-13. Wetting front at 0.01 yr for 1,000-μm
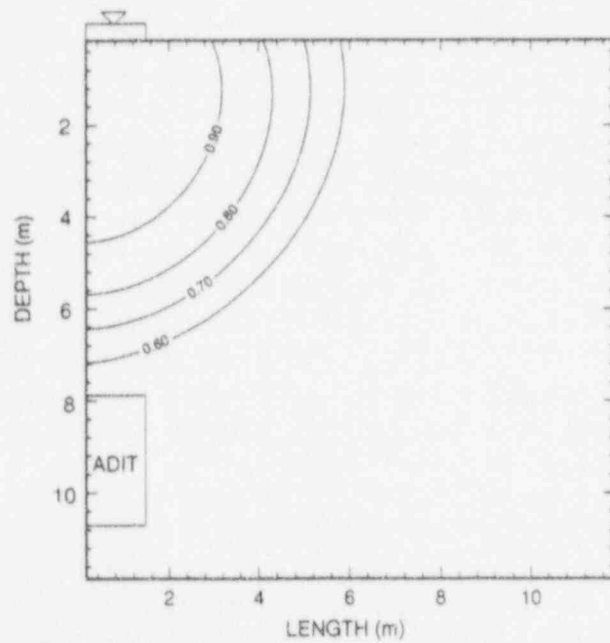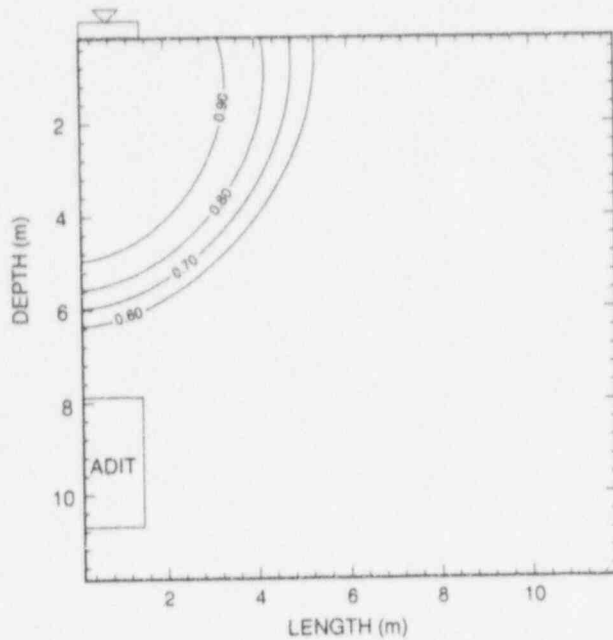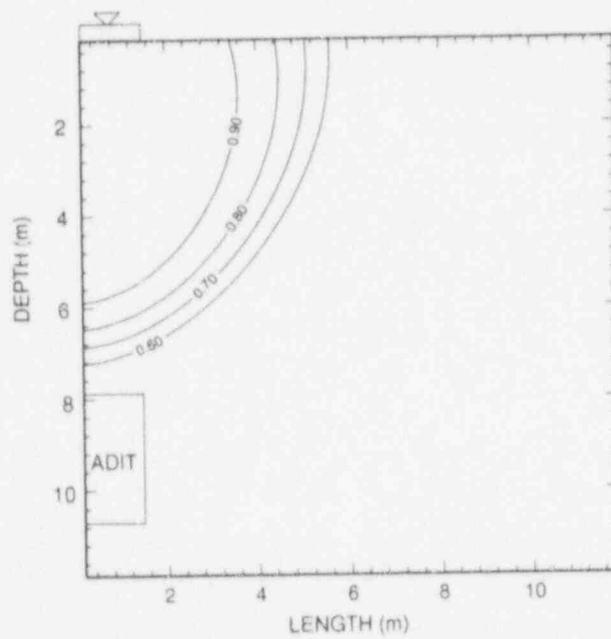fractures in NRG2

NUREG/CR-6356
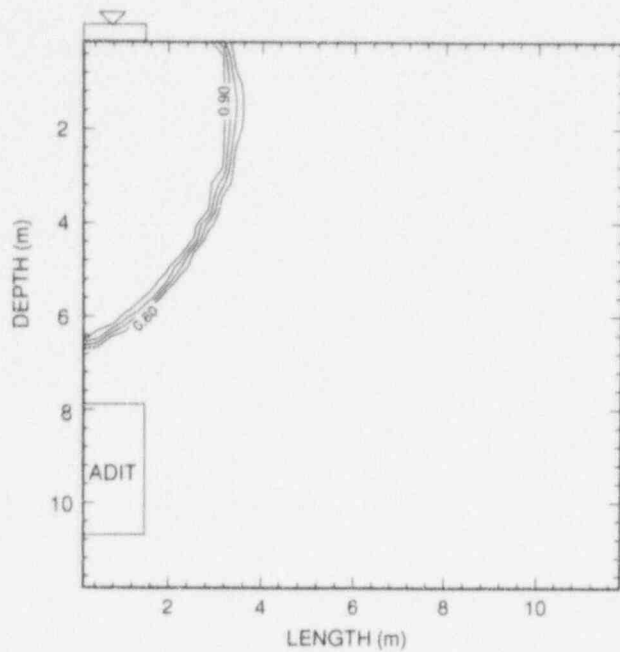
Figure 5-14. Wetting front at 0.002 yr for 1,000-μm fractures in NRG3
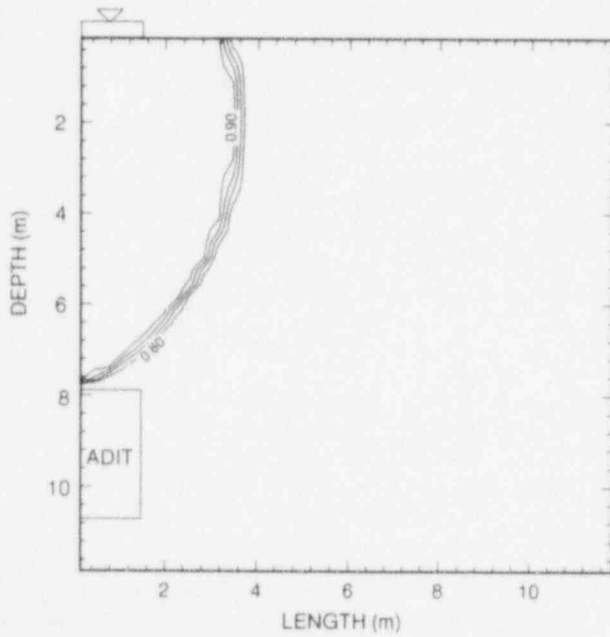
Figure 5-15. Wetting front at 0.005 yr for 1,000-μm fractures in NRG4

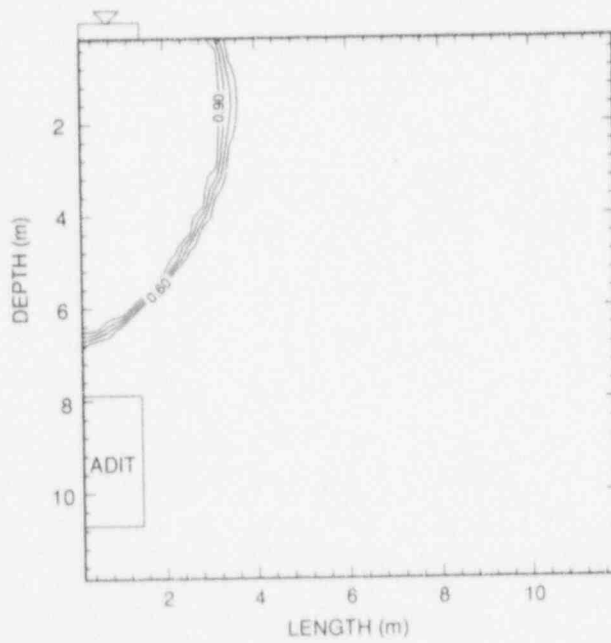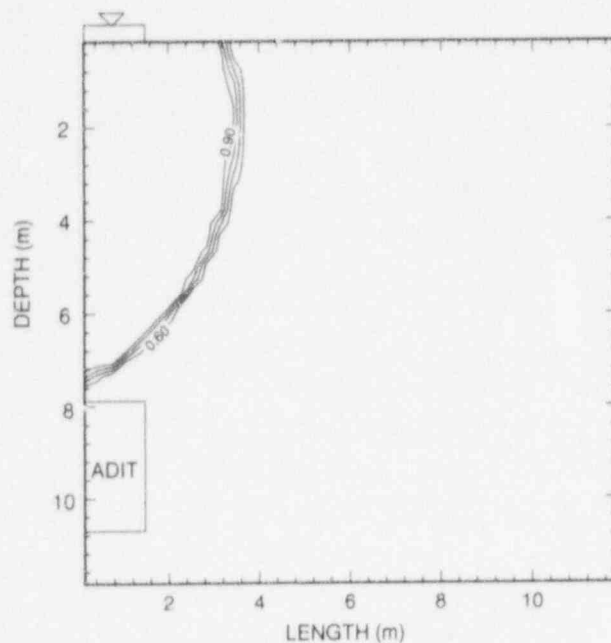**Figure 5-16. Wetting front at 0.008 yr for 1,000-μm fractures in NRG5**

hydraulic conductivity. The 4 day arrival time of water percolating through media with a porosity of 0.29 (NRG1) is approximately double the 2 day arrival time of NRG4 with a porosity of 0.12.

These simulations indicate that predicted arrival times of a wetting front from water introduced at ground surface and detected at a depth of 8 m can vary from a few days to several thousand years for a physical system in which matrix properties are known but fracture characteristics are estimated. Alternative conceptual models not predicated on matrix/fracture hydraulic equilibrium and not assuming uniform, homogeneous media could conceivably provide different wetting front and arrival time predictions. The variety of fracture systems and zones at the Peña Blanca natural analog, if characterized to the degree possible, provides a site in which matrix/fracture percolation tests can be conducted to evaluate the matrix/fracture continuum conceptual model discussed here and other alternative conceptual models using a small-scale field experiment.

6 CONCLUSIONS

Relationships among hydraulic characteristics for tuff samples with variable degrees of hydrothermal alteration have been discerned using laboratory measurements on five variably altered samples of tuff collected at the Peña Blanca natural analog. Rock characteristics determined for subsamples from the five tuff specimens included matrix intrinsic properties (bulk density, specific gravity, and effective porosity) and hydraulic matrix properties (saturated hydraulic conductivity, moisture retention curve, and unsaturated hydraulic conductivity). Rock-specific measurements of matrix intrinsic and hydraulic properties provided a basis for assessments of hydrothermal alteration-induced rock characteristics and relationships among the properties.

The tuff samples were collected at selected distances from the hydrothermal U deposit so that each of the five samples exhibited a different level of hydrothermal alteration. The samples in the order of alteration are NRG1, the most highly altered sample, to samples exhibiting lesser amounts of alteration in the following order NRG2, NRG5, NRG3, and NRG4. The analyses showed little difference in the property values between NRG3 and NRG4, indicating that significant effects exhibited in the rock matrix resulting from hydrothermal alteration associated with the Nopal ore body is restricted to less than 40 m of the boundary of the deposit, the distance of NRG3 from the visible extent of the U deposit. Samples NRG3 and NRG4 are presumed to represent essentially the unaltered host rock. The results of the tested rock samples are summarized below. As illustrated in this summary, hydrothermal activity has significantly altered the intrinsic and hydraulic proportions of the tuff matrix. Although not completely analogous to expected processes at YM, these results indicate that thermal effects can sufficiently alter the rock properties and that representative conceptual models will need to accommodate these potential changes.

Note that in this summary all cited quantities are median values and that NRG1 is representative of the highly altered tuff and samples NRG3 and NRG4 are representative of the mostly unaltered host rock.

- Bulk density varied from 1.845 (g/cm^3) in NRG1 to 2.378 (g/cm^3) in the NRG4

- Apparent specific gravity was invariant in all five samples

- Pycnometric porosity varied from 0.29 in NRG1 to 0.06 in NRG3

- Gravimetric porosity varied from 0.256 in NRG1 to 0.074 in NRG4

- Saturated hydraulic conductivity varied from 1.06×10^{-9} m/s in NRG1 to 7.97×10^{-13} m/s in NRG3

- Calculated van Genuchten α parameter (inverse of the air-entry value) varied slightly from 0.1 m^{-1} in NRG5 to 0.2 m^{-1} in NRG3 and NRG4

- Calculated van Genuchten n parameter varied from 2.0 in NRG1 to 1.3 in NRG4

Limitations in the laboratory determination of moisture retention and saturated hydraulic conductivity in highly welded and altered tuff have been evaluated. Tests on rock samples with relatively low hydraulic conductivities typically required longer times to equilibrate and test. Additionally, larger samples were required for hydraulic conductivity testing to ensure that measurements were not unduly influenced by local occurrences of lithophysae or alteration products.

The van Genuchten α parameter was invariant in the fine Nopal tuff samples. However, a correlation between the van Genuchten n parameter (related to the slope of the retention curve) and saturated hydraulic conductivities for the Nopal rock samples was identified. Typically, a large van Genuchten n value (i.e., a flat retention curve) is observed in media exhibiting a narrow pore-size distribution. Media with a narrow pore-size distribution (i.e., uniformly sized pores) have higher permeabilities than comparable media with a large pore-size distribution. These relationships are supported in the correlation discerned between the van Genuchten n parameter and saturated hydraulic conductivity. In this relationship, the van Genuchten n parameter increases linearly with the log of the median saturated hydraulic conductivity. The general relationship between the van Genuchten n parameter and saturated hydraulic conductivity for the Nopal tuff at the Peña Blanca natural analog has been expressed

$$K_{sat} = 10^{-(4n - 15)} \tag{6-1}$$

Although this relationship is consistent with physical relationships between pore structure and hydraulic conductivity, it is empirically determined using measured quantities. Until additional testing of other rock assemblages is performed to test the generality of this relationship, the utility of this relationship can only be applied to the geophysical area from which the rock testing was based.

This caveat notwithstanding, the defined relationship between the van Genuchten n parameter and saturated hydraulic conductivity in Eq. (6-1) is useful in understanding and characterizing the hydraulic nature of the media at Peña Blanca. Coupling this relationship with the spatial distribution of variably hydrothermally altered tuff allows for insight on site characterization that would otherwise require massive sampling and testing.

Conceptual models of composite fractured porous flow at the Peña Blanca natural analog site have been evaluated. Percolation was simulated using measured matrix properties for samples NRG1 through NRG5 and a range of estimated fracture properties using the numerical simulator C-TOUGH, a modified version of V-TOUGH. Average fracture apertures of 1 to 1,000 μm were assumed in the simulations to assess the impact of fracture aperture on percolation predictions in the composite conceptual model. Several observations are made using these results.

- Predictions of arrival time of the wetting front at the adit vary from less than 2 days through NRG4 with an assumed average fracture aperture of 1,000 μm to about 10,000 yr through the same medium but with apertures of 1 μm.

- Wetting fronts are diffuse for percolation through media dominated by matrix flow but sharp when fractures significantly contribute to flow.

- Arrival times through media with large fractures (i.e., 1,000 μm) are shorter for media with smaller porosities irrespective of the hydraulic conductivity of the medium. For example, the 2-day arrival time for percolation through NRG4 media with a porosity of 0.12 and a hydraulic conductivity of 2.42×10^{-12} m/s is about half the 4-day arrival time for NRG1, which has a porosity of 0.29 and a hydraulic conductivity of 1.06×10^{-9} m/s, both with assumed average fractured apertures of 1,000 μm.

These simulations indicate that predictions of wetting fronts for percolation through fractured porous media from ground surface to a depth of 8 m can vary from a few days to several thousand years. The predicted wetting fronts exhibit distinctly different moisture gradients for the same composite matrix/fracture conceptual model but with different fracture properties. Presumably alternative conceptual models could predict an even wider range of arrival times and moisture gradients. Predictions of percolation presented in this evaluation and assessments of alternative conceptual models could be assessed using results from percolation tests proposed for the Peña Blanca natural analog site.

7 REFERENCES

Alba, L.A., and R. Chavez. 1974. K-Ar ages of volcanic rocks from the central Sierra Peña Blanca, Chihuahua, Mexico. *Isochron West* 10: 21–23.

American Society for Testing Materials. 1977. *Standard Test Method for Specific Gravity and Adsorption of Coarse Aggregate*. Paper No. C-3172-72. Philadelphia, PA: American Society for Testing and Materials: 301–306.

American Society for Testing Materials. 1988. *Standard Test Method for Measurement of Hydraulic Conductivity of Saturated Porous Materials Using a Flexible Wall Permeameter*. Paper No. C-127-88. Philadelphia, PA: American Society for Testing and Materials: 63–68.

American Society for Testing Materials. 1990. *Standard Test Method for Capillary-Moisture Relationships for Fine-Textured Soils by Pressure Membrane Apparatus*. Paper No. C-542-90 Philadelphia, PA: American Society for Testing and Materials: 315–316.

American Society for Testing Materials. 1990. *Standard Test Method for Capillary-Moisture Relationships for Coarse- and Medium-Textured Soils by Pressure Membrane Apparatus*. Paper No. C-5084-90. Philadelphia, PA: American Society for Testing and Materials: 151–158.

American Society for Testing and Materials. 1993. *Standard Test Method for Specific Gravity, Adsorption, and Voids in Hardened Concrete*. Paper No. C-2325-68. Philadelphia, PA: American Society for Testing and Materials: 184–190.

Campbell, J.B. 1991. *AquaLab Model CX-2, Operato⁻'s Manual*. Pullman, WA: Decagon Devices Inc.

Carrier, D.L. 1979. *Gravity and Heat Flow Studies at Twin Peaks: An Area of Late Tertiary Silicic Volcanism in Millard County, Utah*. M.S. Thesis. Salt Lake City, UT: University of Utah.

Danielson, R.E., and P.L. Southerland. 1986. Porosity. *Methods of Soil Analysis Part 1- Physical and Mineralogical Methods*. A. Klute, ed. Madison, WI: Soil Science Society of America, Inc: 443–461.

Domenico, P.A., and F.W. Schwartz. 1990. *Physical and Chemical Hydrogeology*. New York, NY: John Wiley & Sons.

Electric Power Research Institute. 1990. *Demonstration of a Risk-Based Approach to High-Level Waste Repository Evaluations*. EPRI NP-7057. Palo Alto, CA: Electric Power Research Institute.

Electric Power Research Institute. 1992. *Demonstration of a Risk-Based Approach to High-Level Waste Repository Evaluations: Phase 2*. EPRI TR-100384. Palo Alto, CA: Electric Power Research Institute.

Flint, A.L., M.H. Nash, and M.S. Nash. 1994. Hydrologic property alteration due to elevated temperatures at Yucca Mountain. *Proceedings of the Fifth International Conference on High-Level Radioactive Waste Management*. La Grange Park, IL: American Nuclear Society.

Freeze, R.A. 1991. Hydrogeologic issues at Yucca Mountain: Findings of a DOE peer review team. *Proceedings of Workshop V: Flow and Transport Through Unsaturated Fractured Rock-Related to High-Level Radioactive Waste Disposal*. NUREG/CP-0040. Washington, DC: Nuclear Regulatory Commission.

Freeze, R.A., and J.A. Cherry. 1979. *Groundwater*. Englewood Cliffs, NJ: Prentice-Hall, Inc.: 18–45.

Gee, G.W., M.D. Campbell, G.S. Campbell, and J.H. Campbell. 1992. Rapid measurement of low soil water potentials using a water activity meter. *Soil Science of America Journal* 56: 1,068–1,072.

George-Aniel, B., J.L. Leroy, and B. Poty. 1991. Volcanogenic U mineralization of the Sierra de Peña Blanca district, Chihuahua, Mexico: Three genetic models. *Economic Geology* 86: 233–248.

Goodell, P.C. 1981. Geology of the Pena Blanca uranium deposits, Chihuahua, Mexico. *U in Volcanic and Volcaniclastic Rocks–AAPG Studies in Geology No. 13*. P.C. Goodell and A.C. Waters, eds. El Paso, TX: American Association of Petroleum Geologists: 275–291

Hillel, D. 1971. *Soil and Water*. New York City, NY: Academic Press: 29–127.

Ildefonse, P., J.-P. Muller, B. Clozel, and G. Calas. 1990. Study of two alteration systems as natural analogues for radionuclide release and migration. *Engineering Geology* 29: 413–439.

Kapoor, V. 1994. *Water Film Flow in a Fracture in Unsaturated Porous Medium*. CNWRA 94-009. San Antonio, TX: Center for Nuclear Waste Regulatory Analyses.

Klavetter, E.A., and Peters, R.R. 1986. *Estimation of Hydrologic Properties of an Unsaturated, Fractured Rock Mass*. SAND84-2642. Albuquerque, NM: Sandia National Laboratory.

Klute, A. 1986. *Water Retention: Laboratory Methods*. A. Klute, ed. Madison Soil Science Society of America, Inc. Madison, WI: American Society of Agronomy, Inc.: 635–662.

Krynine, D.P., and W.R. Judd. 1951. *Principles of Engineering Geology and Geotechnics*. New York City, NY. McGraw Hill: 46–50.

Marshall, T.J., and J.W. Holmes. 1988. *Soil Physics*. Cambridge, England: Cambridge University Press: 1–81.

Mohanty, S. 1994. *Single Fracture Flow Behavior of Apache Leap Tuff Under Normal and Shear Loads*. CNWRA 94-024. San Antonio, TX: Center for Nuclear Waste Regulatory Analyses.

Mualem, Y. 1976. A new model predicting the hydraulic conductivity of unsaturated porous materials. *Water Resources Research* 12(3): 513–522.

Murphy, W.M., and E.C. Pearcy. 1992. Source-term constraints for the proposed repository at Yucca Mountain, Nevada, derived from the natural analog at Peña Blanca. Mexico. *Symposium Proceedings of the Scientific Basis for Nuclear Waste management XV.* C.G. Sombret, ed. Pittsburgh, PA: Materials Research Society 257: 521–527.

Nitao, J.J. 1988. *Numerical Modeling of the Thermal and Hydrological Environment Around a Nuclear Waste Package Using the Equivalent Continuum Approximation: Horizontal Emplacement.* UCID-21444. Livermore, CA: Lawrence Livermore National Laboratory.

Nitao, J.J. 1989. V-TOUGH—*An Enhanced Version of the TOUGH Code for the Thermal and Hydrologic Simulation of Large-Scale Problems in Nuclear Waste Isolation.* UCID-21954. Livermore, CA: Lawrence Livermore National Laboratory.

Page, J.B. 1948. Advantages of the pressure pycnometer for measuring the pore space in soils. *Proceedings - Soil Science Society of America* 12: 81–84.

Pearcy, E.C. 1994. *Fracture Transport of Uranium at the Nopal I Natural Analog Site.* CNWRA 94-011. San Antonio, TX: Center for Nuclear Waste Regulatory Analyses.

Pearcy, E.C., and W.M. Murphy. 1992. *Geochemical Natural Analogs Literature Review.* CNWRA 90-008. San Antonio, TX: Center for Nuclear Waste Regulatory Analyses.

Pearcy, E.C., and W.M. Murphy. 1992. *Site Selection and Workplan Report for the Geochemical Natural Analog Research Project.* CNWRA 92-014. San Antonio, TX: Center for Nuclear Waste Regulatory Analyses.

Pearcy, E.C., J.D. Prikryl, W.M. Murphy, and B.W. Leslie. 1993. *U mineralogy of the Nopal I Natural Analog Site, Chihuahua, Mexico.* CNWRA 93-012. San Antonio, TX: Center for Nuclear Waste Regulatory Analyses.

Pearcy, E.C., J.D. Prikryl, W.M. Murphy, and B.W. Leslie. 1994. Alteration of uraninite from the Nopal I deposit, Peña Blanca, District, Chihuahua, Mexico, compared to degradation of spent nuclear fuel in the proposed US high-level nuclear waste repository at Yucca Mountain, Nevada. *Journal of Applied Geochemistry* 9: 713–732.

Pruess, K. 1987. *TOUGH User's Guide.* NUREG/CR-4645. Berkeley, CA: Lawrence Berkeley Laboratory.

Rasmussen, T.C., D.D. Evans, P.J. Sheets, and J.H. Blanford. 1990. *Unsaturated Fractured Rock Characterization Methods and Data Sets at the Apache Leap Tuff Site.* NUREG/CR-5596. Washington DC: Nuclear Regulatory Commission.

Russell, M.B. 1950. A simplified air-pycnometer for field use. *Proceedings - Soil Science Society of America* 14: 73–76.

Russel, C.E., J.W. Hess, and S.W. Tyler. 1987. Hydrogeologic investigations of flow in fractured tuffs, Rainer Mesa, Nevada test site. Flow and transport through unsaturated fractured rock. D.D. Evans and T.J. Nicholson, eds. Washington, DC: *American Geophysical Union*: 43–50.

Sandia National Laboratories. 1992. *TSPA 1991: An Initial Total-System Performance Assessment for Yucca Mountain.* SAND 91-2795. Albuquerque, NM: Sandia National Laboratories.

Sandia National Laboratories. 1994. *Total-Systems Performance Assessment for Yucca Mountain—SNL Second Iteration (TSPA–1993).* SAND 93-2675. Albuquerque, NM: Sandia National Laboratories.

Snow, D.T. 1968. Rock fracture spacings, openings, and porosities. Journal of Soil Mechanics Foundation Division. *Proceedings of American Society Civil Engineers* 94: 73–91.

Sowers, G.F. 1979. *Introductory Soil Mechanics and Foundation Geotechnical Engineering.* 4th ed. New York, NY: MacMullin.

U.S. Nuclear Regulatory Commission. 1992. *Initial Demonstration of the NRC's Capability to Conduct a Performance Assessment for a High-Level Waste Repository.* NUREG-1327. Washington, DC: U.S. Nuclear Regulatory Commission.

U.S. Nuclear Regulatory Commission. 1993. *Draft License Application Review Plan for the Review of a License Application for a Geologic Repository for Spent Nuclear Fuel and High-Level Radioactive Waste Yucca Mountain Site, Nevada.* NUREG-1323. Washington, DC: U.S. Nuclear Regulatory Commission.

U.S. Nuclear Regulatory Commission. 1994. *License Application Review Plan for a Geologic Repository for Spent Nuclear Fuel and High-Level Radioactive Waste.* NUREG-1323. Rev. 0. Washington, DC: U.S. Nuclear Regulatory Commission.

U.S. Nuclear Regulatory Commission. 1995. *Phase 2 Demonstration of the NRC's Capabilities to Conduct a Performance Assessment for a High-Level Waste Repository.* NUREG-1464. Washington, DC: U.S. Nuclear Regulatory Commission.

U.S. Environmental Protection Agency. 1989. *Environmental Radiation Protection Standards for Management and Disposal of Spent Nuclear Fuel, High-Level and Transuranic Radioactive Wastes.* Title 40, Protection of the Environment, Part 191. Washington, DC: U.S. Government Printing Office.

van Genuchten, M.Th. 1980. A Closed-form equation for predicting the hydraulic conductivity of unsaturated soils. *Soil Science of America Journal* 44: 892–898.

van Genuchten, M.Th., F.J. Leih, and S.R. Yates. 1991. *The RETC Code for Quantifying the Hydraulic Functions of Unsaturated Soils.* Riverside, CA: Environmental Research Laboratory, U.S. Environmental Protection Agency.

Wang, J.S.Y. 1992. Variations of hydrological parameters of tuff and soil. *Proceedings of the Third International Conference on High-Level Radioactive Waste Management*. La Grange Park, IL: American Society of Civil Engineers.

Wang, J.S.Y., and T.N. Narasimhan. 1986. *Hydrologic Mechanisms Governing Partially Saturated Fluid Flow in Fractured Welded Units and Porous Nonwelded Units at Yucca Mountain*. LBL-21022. Berkeley, CA: Lawrence Berkeley Laboratory.

2. TITLE AND SUBTITLE Hydraulic Characterization of Hydrothermally Altered Nopal Tuff	
	3. DATE REPORT PUBLISHED
	MONTH: July YEAR: 1995
	4. FIN OR GRANT NUMBER B6666

5. AUTHOR(S) R.T. Green, G. Rice*, K.A. Meyer-James	6. TYPE OF REPORT
	7. PERIOD COVERED *(Inclusive Dates)*

8. PERFORMING ORGANIZATION – NAME AND ADDRESS *(If NRC, provide Division, Office or Region, U.S. Nuclear Regulatory Commission, and mailing address; if contractor, provide name and mailing address.)*

Southwest Research Institute   * Consultant
Center for Nuclear Waste Regulatory Analyses   George Rice and Associates
6220 Culebra Road   San Antonio, TX
San Antonio, TX 78228-0510

9. SPONSORING ORGANIZATION – NAME AND ADDRESS *(If NRC, type "Same as above"; if contractor, provide NRC Division, Office or Region, U.S. Nuclear Regulatory Commission, and mailing address.)*

Division of Regulatory Applications
Office of Nuclear Regulatory Research
U.S. Nuclear Regulatory Commission
Washington, DC 20555-0001

10. SUPPLEMENTARY NOTES

11. ABSTRACT *(200 words or less)*

Understanding the mechanics of variably saturated flow in fractured-porous media is of fundamental importance to evaluating the isolation performance of the proposed high-level radioactive waste repository for the Yucca Mountain site. Developing that understanding must be founded on the analysis and interpretation of laboratory and field data. This report presents an analysis of the unsaturated hydraulic properties of tuff cores from the Peña Blanca natural analog site in Mexico. The basic intent of the analysis was to examine possible trends and relationships between the hydraulic properties and the degree of hydrothermal alteration exhibited by the tuff samples. These data were used in flow simulations to evaluate the significance of a particular conceptual (composite) model and of distinct hydraulic properties on the rate and nature of water flow.

| 12. KEY WORDS/DESCRIPTORS *(List words or phrases that will assist researchers in locating the report.)* hydrothermally altered tuff, high-level waste geologic repository, hydraulic characterization of unsaturated rock, van Genuchten parameters, composite medium, infiltration	13. AVAILABILITY STATEMENT unlimited
	14. SECURITY CLASSIFICATION *(This Page)* unclassified *(This Report)* unclassified
	15. NUMBER OF PAGES
	16. PRICE

Printed
on recycled
paper
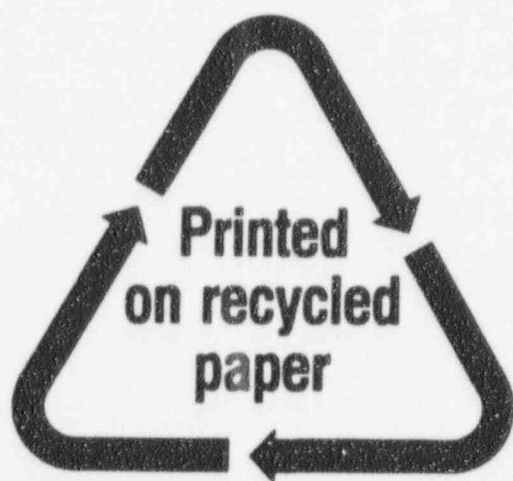
Federal Recycling Program

HYDRAULIC CHARACTERIZATION OF
HYDROTHERMALLY-ALTERED NOPAL TUFF

DECEMBER 1994

NUREG/CR-6356

UNITED STATES
NUCLEAR REGULATORY COMMISSION
WASHINGTON, DC 20555-0001

———

OFFICIAL BUSINESS
PENALTY FOR PRIVATE USE, $300

120555139531   1 1AN1RW
US NRC-OADM
DIV FOIA & PUBLICATIONS SVCS
TPS-PDR-NUREG
2WFN-6E7
WASHINGTON   DC   20555